Microscopic character of the Lower Cretaceous Tuxen and Sola formations in the Boje-2C well, Danish Central Graben

IDA L. FABRICIUS, MORTEN L. HJULER, MADS E. JELBY & KRESTEN ANDERSKOUV

Geological Society of Denmark
https://2dgf.dk

Received 20 December 2024
Accepted in revised form 12 June 2025
Published online 20 October 2025

© 2025 the authors. Re-use of material is permitted, provided this work is cited. Creative Commons License CC BY: https://creativecommons.org/licenses/by/4.0/

Fabricius, I.L., Hjuler, M.L., Jelby, M.E. & Anderskouv, K. 2025. Microscopic character of the Lower Cretaceous Tuxen and Sola formations in the Boje-2C well, Danish Central Graben. Bulletin of the Geological Society of Denmark, Vol. 71, pp. 127–162. ISSN 2245-7070. https://doi.org/10.37570/bgsd-2025-71-08

The Lower Cretaceous Tuxen and Sola formations in the Danish Central Graben (North Sea) constitute pelagic chalks and marlstones, which locally are hydrocarbon-bearing. Based on previous identification of 21 sedimentary facies in the cored Boje-2C well of the Boje Field, 66 samples were analysed through backscattered electron microscopy to delineate how the microscopic character reflects the macroscopic sedimentary facies and to identify indications of diagenesis. For most samples, microscopic characters can clearly be related to the previously identified sedimentary facies. Bioturbation and shear deformation, however, were not consistently reflected in the microscopic character. In all samples, the microtexture is characterised by massive or laminated calcareous mudstone with varying content of mainly kaolinitic clay and only sparse remains of microfossils or shell fragments, whereas particles of quartz silt and kaolinitic claystone silt are common. Porosity is mainly interparticular, typically reaching 25% in the Sola and upper Tuxen formations, and declining with depth to ca. 17% in the lower Tuxen and upper Valhall formations. Diagenesis is reflected in the occurrence of calcite cementation, pyrite and calcite-rimmed dolomite, and some pores may represent moulds after silicious microfossil fragments, which probably sourced the locally observed silicification of the sediment. Further, in clay-poor intervals below the oil zone, a significant diagenetic feature constitutes biogenic calcite mud particles that become increasingly recrystallized and euhedral with depth. It is therefore possible that burial-related crystal ripening was delayed in the oil zone represented by the upper part of the core. In the underlying transition zone, which in the Boje-2C well comprises most of the Tuxen Formation, the degree of recrystallization increases with depth as water saturation increases. Pressure dissolution features were noted in clay-rich intervals, but proper stylolites were not encountered, reflecting the generally high clay content of these marly chalks.

Keywords. Aptian, Barremian, chalk, diagenesis, marlstone, SEM

Ida L. Fabricius [ilfa@dtu.dk] and Morten L. Hjuler, Department of Environmental and Resource Engineering, Technical University of Denmark, Denmark. Mads E. Jelby [jelby@geo.au.dk], Department of Geoscience, Aarhus University, Aarhus, Denmark. Kresten Anderskouv [ka@ign.ku.dk], Department of Geosciences and Natural Resource Management, University of Copenhagen, Denmark

Inferences of the depositional history of pelagic carbonates are largely based on macroscopic features, whereas rock properties are mainly controlled by features that can only be observed microscopically. The relation between microscopic features and depositional (macroscopic) facies in the Lower Cretaceous chalk and marlstone of the Tuxen and Sola formations in the Danish Central Graben (DCG), North Sea, has not been presented in detail. Herein, a systematic analysis of the microscopic character of macroscopically identified pelagic carbonate facies is presented as a case study, utilizing the cored section of the Boje-2C well in the central part of the DCG.

The Lower Cretaceous succession in the DCG is largely encompassed by the Cromer Knoll Group, an up to one kilometre thick succession of siliciclastic mudstone, marlstone and chalk of predominantly hemipelagic and pelagic origin (Figs 1A, 2; Copestake *et al.* 2003; Mutterlose & Bottini 2013; van Buchem *et al.* 2018). Initial exploration-related drilling campaigns in the DCG (e.g. Damtoft *et al.* 1992) led to the recognition of the Lower Cretaceous chalk

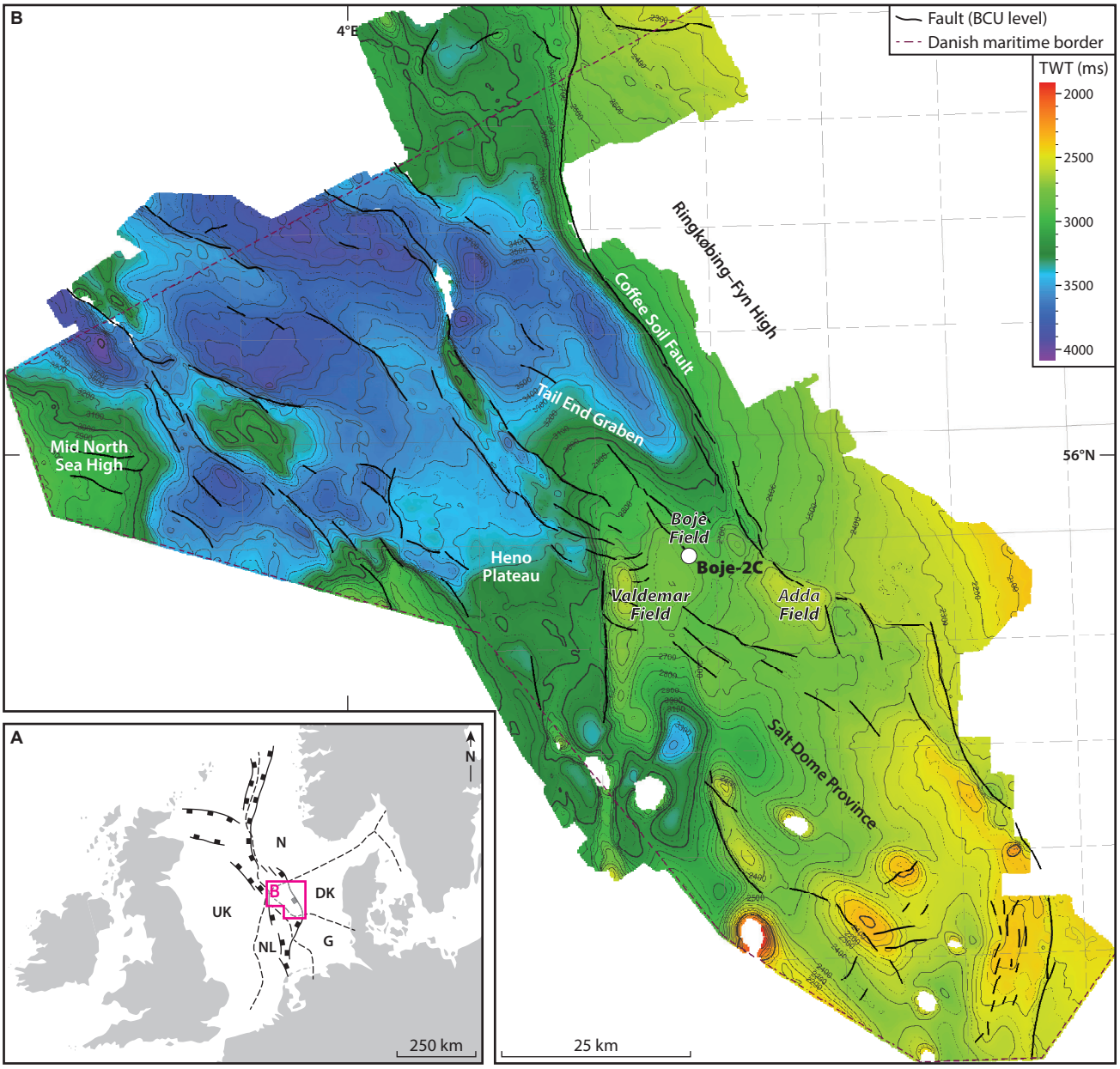


Fig. 1. A. Simplified structural configuration of the larger North Sea Basin (modified from Japsen *et al.* 2003; Møller & Rasmussen 2003), indicating the Danish (DK), German (G), Norwegian (N), Dutch (NL) and United Kingdom (UK) sectors of the Central Graben. **B**. Time-structure map (two-way travel time (TWT)) of the Base Cretaceous Unconformity (BCU), indicating the position of the Boje-2C well in the Boje Field located between the Valdemar Field and Adda Field (modified from Jelby *et al.* 2024, based on Ineson *et al.* 2022b).

succession as a potential reservoir, and with the Tuxen and overlying Sola formations (Hauterivian–Albian) being oil-bearing, the Valdemar Field and adjacent Adda Field were declared commercial (Fig. 1B; Ineson 1993). Consequently, these formations have been repeatedly drilled, geophysically logged, cored, and described with different focus, notably including: reservoir properties (Jakobsen *et al.* 2004, 2005; Fabricius *et al.* 2005; Storebø *et al.* 2022a, b; Meireles & Fabricius 2023); mineralogy, palaeoenvironment and palaeoclimate (Blok *et al.* 2022, 2023); fractures (Glad *et al.* 2022); as well as sedimentology and facies architecture (Michelsen *et al.* 1987; Ineson 1993; Ineson *et al.* 2022a; Jelby *et al.* 2022, 2024).

The oil-bearing well Boje-2C was drilled in 2013 in the Boje Field situated between the Adda and Valdemar fields (Fig. 1B). Interpretation of log and core data from the Tuxen and Sola formations indicates porosity in the range of 20–30% and permeability in the range of 0.01–1 mD (Storebø *et al.* 2022a, b). The specific surface area with reference to bulk volume varies from 10 to 40 m^2/cm^3, thus, although water saturation varies

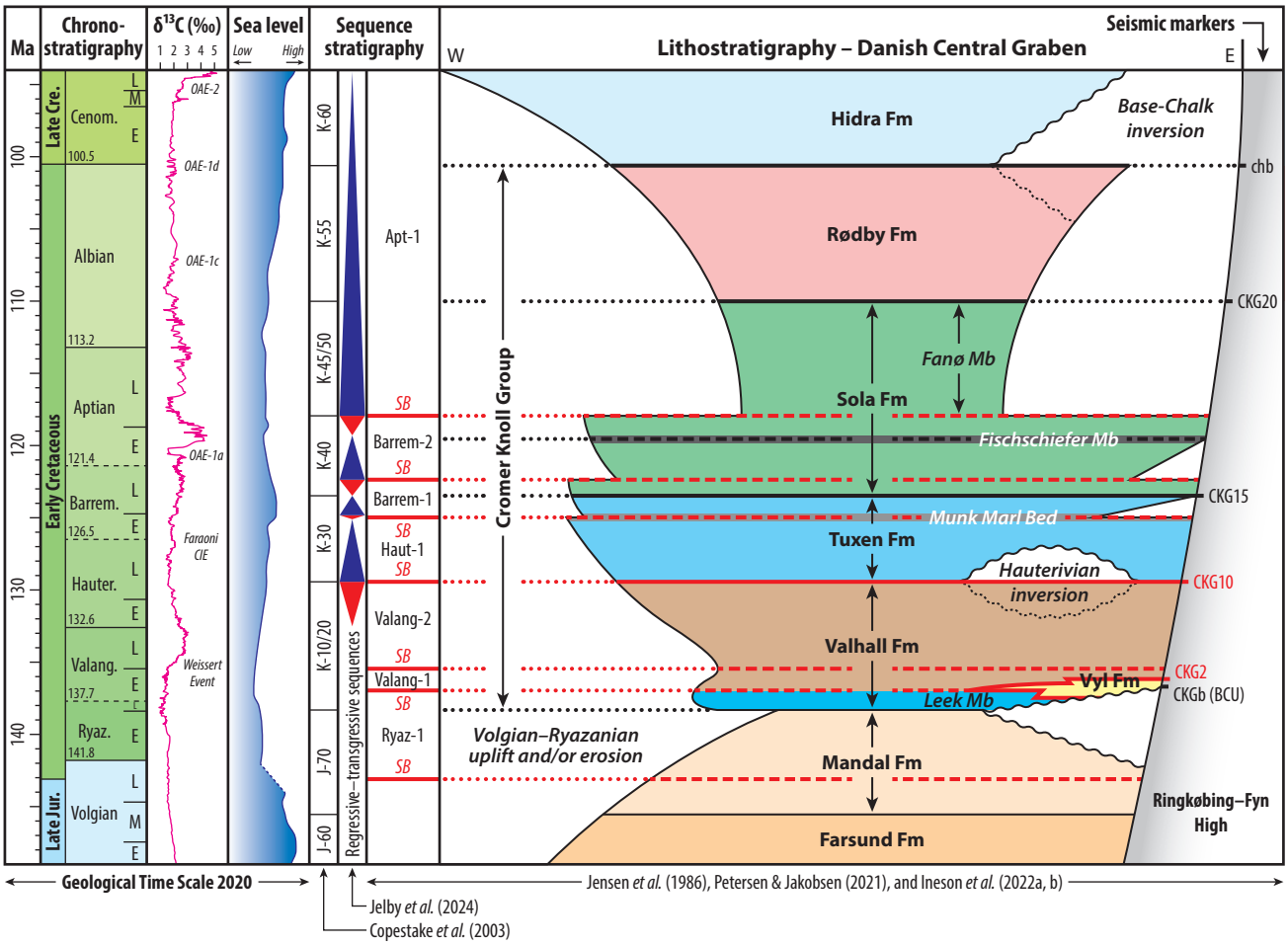


Fig. 2. Stratigraphic summary chart of the Danish Central Graben, showing the gross relative lateral distribution, sequence stratigraphic models of previous key studies, and key seismic horizons of the Lower Cretaceous Cromer Knoll Group in a W–E-oriented cross-section, compiled from Jensen *et al.* (1986), Petersen & Jakobsen (2021), Ineson *et al.* (2022a, b), and Jelby *et al.* (2024). Numerical ages, chronostratigraphy, stable carbon-isotope ($\delta^{13}C$) stratigraphy and events, as well as sea-level curve are compiled from Gale *et al.* (2020) and Hesselbo *et al.* (2020). BCU, Base Cretaceous Unconformity; SB, sequence boundary.

through the section, water is interpreted to be irreducible down to the upper part of the Tuxen Formation. Accordingly, no indication of compartmentalization has been reported (Storebø *et al.* 2022a, b).

Palaeoenvironmental studies indicate that deposition took place at ~46°N in a sub-photic, epicontinental ramp setting as part of the larger Euro-Boreal Realm (Blok *et al.* 2022; Jelby *et al.* 2024). Blok *et al.* (2022, 2023) found that the main mineralogical component of the succession is calcite with co-varying constituents of quartz and kaolinite clay indicating a detrital source from exposed continental rock, possibly in the form of nearby islands. The relative proportion of calcite and siliciclastic material varies stratigraphically, reflecting variation in pelagic carbonate production and continental runoff. Minor mineralogical constituents include illite, smectite-illite, and chlorite, while pyrite, dolomite, siderite and goethite occur locally (Blok *et al.* 2022, 2023).

With respect to post-depositional deformation, thin inclined deformation (compaction) bands and shear fractures have been noted in both the Boje-2C and other cores from the Valdemar Field (Glad *et al.* 2022; Jelby *et al.* 2022). Flaser lamination (*sensu lato* solution seams; Garrison & Kennedy 1977) have also been noted in chalk-dominated divisions, but no proper stylolites were reported.

Jelby *et al.* (2022) provided a detailed sedimentological description of several cored wells, including Boje-2C (Fig. 3). In addition to a minor occurrence of volcanic tuff, the authors identified five chalk–marlstone lithologies and seven different sedimentary structures or fabrics. In the Boje-2C core, the combination of the lithologies and sedimentary structures represents 21 facies, of which 18 are described herein with focus on their corresponding microscopic character (Tables 1, 2).

Thus, the primary aim of the present study is to

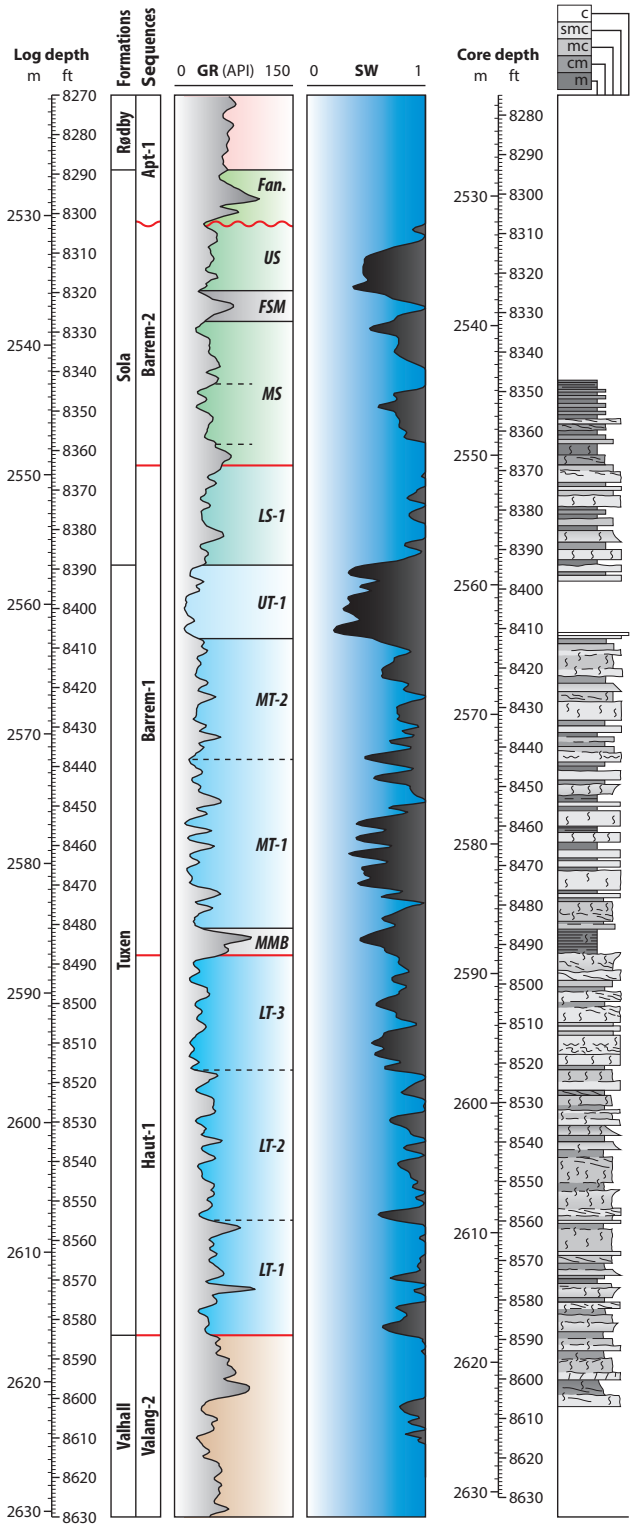


Fig. 3. Sedimentological and gamma-ray (GR) logs, water saturation (SW) log (Meireles & Fabricius 2023), reservoir zones (Jakobsen *et al.* 2004) and depositional sequences (Ineson *et al.* 2022a, b) in the Boje-2C well (modified from Jelby *et al.* 2022, 2024). The core:log depths are shifted with ~5 ft. Red straight and wavy lines are conformable and unconformable sequence boundaries, respectively. Reservoir -zone abbreviations refer to: LT 1–3, Lower Tuxen 1–3; MMB, Munk Marl Bed; MT 1–2, Middle Tuxen 1–2; UT-1, Upper Tuxen-1; LS-1, Lower Sola-1; MS, Middle Sola; FSM, Fischschiefer Member; US, Upper Sola; Fan., Fanø Member. Lithological abbreviations refer to: c, chalk; smc, slightly marly chalk; mc, marly chalk; cm, chalky marlstone; m, marlstone.

document the microscopic character of facies in the Tuxen and Sola formations in the Boje-2C core. Subordinately, the sedimentary and diagenetic processes that have resulted in the observed microscopic character are discussed, with special emphasis on potential links between macro- and microscopic features and the cause for depth-dependant variation.

Regional setting and stratigraphy

In the Early Cretaceous, the North Sea Basin (Fig. 1A) formed part of a regionally extensive, but enclosed, epicontinental sea with a general low-gradient ramp physiography dissected centrally by a N–S-trending deeper-water graben system, including the DCG. The basin had relatively narrow connections to the open ocean to the north, and progressively to the south during post-Barremian times. Prior to the Aptian, however, the southern margin of the basin was closed off from Tethyan influence (Tyson & Funnell 1987; Mutterlose 1992; Ineson 1993). The DCG consists of a complex series of NNW–SSE-trending half-grabens bounded by the Coffee Soil Fault and Ringkøbing–Fyn High to the east and by the Mid North Sea High to the west (Fig. 1B; e.g. Japsen *et al.* 2003). Formation of the DCG commenced during repeated regional rifting and corresponding fault-controlled subsidence, which was initiated in the Callovian and continued into the Ryazanian (Møller & Rasmussen 2003). In the Early Cretaceous, the active rift phase was replaced by regional thermal subsidence centred on the axial graben system of the DCG, although differential subsidence of Late Jurassic half-grabens persisted from the Ryazanian to the mid-Hauterivian but decreased into the late Hauterivian (Vejbæk 1986; Vejbæk & Andersen 1987).

The Tuxen Formation (lower Hauterivian – upper Barremian) is ~20–80 m (65–260 ft) thick in the DCG (Jensen *et al.* 1986). The formation predominantly consists of white to off-white intensely bioturbated and commonly argillaceous nannofossil chalk interbedded with bioturbated to laminated grey to green-grey marlstone (Fig. 3) of inferred pelagic and hemipelagic origin (Ineson 1993; Jelby *et al.* 2022).

The formation is characterised by two discrete chalk-dominated units separated by an up to 2 m (7 ft) thick unit of dark-grey to black, laminated, organic-rich marlstone of early Barremian age, named the 'Munk

Table 1. List of studied samples. Depth has reference to core and indicates lowermost part of sample

Stratigraphy	Sample ID	Facies
Middle Sola Formation	Bj-2G8348'4" *	5 c
	Bj-2G8350'5" *	4 y
	Bj-2G8352'1" *	4 c
	Bj-2G8369'1"	4 b
Lower Sola Formation	Bj-2G8369'11"	3 b
	Bj-2G8377'2" *	2 z
	Bj-2G8379'11"	2 a
	Bj-2G8381'11" *	5 a
	Bj-2G8385'11" *	5 y
	Bj-2G8388'4" *	5 b
	Bj-2G8390'1" *	2 b
	Bj-2G8393'11" *	5 c
Upper Tuxen Formation	Bj-2G8411'2"	1 a
Middle Tuxen Formation	Bj-2G8413'1"	2 y
	Bj-2G8416'0"	5 b
	Bj-2G8424'11"	3 b
	Bj-2G8430'11"	2 b
	Bj-2G8433'1"	2 b
	Bj-2G8444'11"	2 x
	Bj-2G8446'3" *	5 c
	Bj-2G8450'11" *	3 b
	Bj-2G8451'11" *	3 b
	Bj-2G8456'11" *	2 a
	Bj-2G8459'10" *	2 b
	Bj-2G8469'5" *	2 a
	Bj-2G8472'0"	2 b
	Bj-2G8475'11"	4 a
	Bj-2G8478'3"	1 a
	Bj-2G8480'3" *	3 b
	Bj-2G8485'0" *	3 b
Munk Marl Bed	Bj-2G8486'0" *	5 c
	Bj-2G8487'1" *	5 c
	Bj-2G8488'4" *	5 c
	Bj-2G8488'11" *	5 c
	Bj-2G8490'3"	5 c
	Bj-2G8491'1"	5 c
Lower Tuxen Formation	Bj-2G8491'11"	4 b
	Bj-2G8492'11"	2 b
	Bj-2G8494'1"	2 z
	Bj-2G8495'1"	3 z
	Bj-2G8505'0" *	2 b
	Bj-2G8511'1"	2 b
	Bj-2G8512'9"	2 b
	Bj-2G8515'2"	2 y
	Bj-2G8520'0" *	2 a
	Bj-2G8526'11" *	3 y
	Bj-2G8532'4"	4 a
	Bj-2G8536'0"	3 a
	Bj-2G8539'5" *	4 a
	Bj-2G8541'11" *	2 z
	Bj-2G8550'5" *	2 b
	Bj-2G8557'11"	2 y
	Bj-2G8559'1"	3 b
	Bj-2G8560'0" *	2 b
	Bj-2G8566'1" *	3 b
	Bj-2G8568'8" *	3 b
	Bj-2G8574'1" *	2 b
	Bj-2G8574'10" *	2 a
	Bj-2G8576'1"	3 a
	Bj-2G8579'0" *	3 a
	Bj-2G8581'1"	2 y
	Bj-2G8582'0" *	2 y
	Bj-2G8582'4"	4 a
	Bj-2G8586'0"	2 a
Valhall Formation	Bj-2G8604'2" *	4 b
	Bj-2G8607'0"	2 a

*Samples where mineralogy is confirmed by Energy Dispersive Spectrometry.

Marl Bed' (Jensen *et al.* 1986). The carbonate content of the formation overall increases upwards with the cleanest chalk and best reservoir quality observed in the top of the succession, as indicated by a low, blocky gamma-ray response (Fig. 3; Kühnau & Michelsen 1994; Jakobsen *et al.* 2004; Jelby *et al.* 2022, 2024).

The Sola Formation (upper Barremian – Albian) is ~20–40 m (65–130 ft) thick in the DCG (Jensen *et al.* 1986). The formation generally displays a heterogeneous, and compared to the Tuxen Formation, more marly facies development of mainly grey-green to buff marlstone and claystone, dark-grey to black laminated marlstone and claystone (Fig. 3), as well as pale chalk and argillaceous chalk, and local siltstone and sandstone (Jensen & Buchardt 1987; Ineson 1993; Jelby *et al.* 2022). Alternating pelagic and hemipelagic processes thus dominated deposition, with fluctuation of bottom-water oxygen levels and terrestrially derived sediment input (Jensen & Buchardt 1987; Jelby *et al.* 2022, 2024).

Material and methods

A total of 66 samples from the uppermost Valhall, Tuxen and Sola formations in the Boje-2C core were analysed for their microscopic character (Table 1). The samples were cleaned for pore water-derived salt and for hydrocarbons by reflux with methanol and toluene in a Soxhlet setup; impregnated with epoxy resin; and vertically oriented polished sections were subsequently prepared. Each section was coated with a 7–30 nm thick carbon film to avoid charging issues, and backscattered electron (BSE) images were recorded by an FEI Quanta 200 scanning electron microscope (SEM) equipped with an energy-dispersive X-ray spectrometer (EDS) (X-max 150, Oxford Instruments) at DTU Sustain, Technical University of Denmark. For each sample, several BSE images were taken, herein represented by one image of the texture and one image of the pore structure for each sample (Figs 4–15; A1–A5). Further, identification of the mineralogical content of each sample was aided by extensive EDS analyses of 36 samples (Table 1). The facies are annotated according to Jelby *et al.* (2022). Due to the original well and core depths being reported in imperial units, both these and converted metric units are used throughout this paper.

Microscopic character of facies

Facies 1a. *Homogeneously bioturbated chalk*

This facies is represented by two samples from the Tuxen Formation (Fig. 4; Table 2). Both samples display massive carbonate mudstone with contact ce-

Table 2. Combinations of lithology and fabric in cores from well Boje-2C (Jelby *et al.* 2022)

		Lithology				
		1 Chalk	2 Slightly marly chalk	3 Marly chalk	4 Chalky marlstone	5 Marlstone
Fabric						
a	Homogenous bioturbation	Tuxen (2)	Sola (1) Tuxen (5) Valhall (1)	Tuxen (3)	Tuxen (4)	Sola (1)
b	Mottled bioturbation		Sola (1) Tuxen (11)	Sola (1) Tuxen (8)	Sola (1) Tuxen (1) Valhall (1)	Sola (1) Tuxen (1)
c	Parallel lamination				Sola (1)	Sola (2) Tuxen (1) Munk Marl (6)
x	Flaser lamination		Tuxen (1)			
y	Shear deformation structures		Tuxen (5)	Tuxen (1)	Sola (1)	Sola (1)
z	Silicified fabric		Sola (1) Tuxen (2)	Tuxen (1)		

Formation name indicates where each combination is found and number of samples is given in parantheses. In addition to the Sola and Tuxen formations, also the deeper Valhall Formation is represented.

mentation among the recrystallized particles. The pore space is predominantly inter-particulate with maximal pore diameter less than five microns. The upper sample appears relatively less cemented and contains identifiable nannoconids and sparse diagenetically altered microfossils, one with pore-filling pyrite.

Facies 2a. *Homogeneously bioturbated slightly marly chalk*

This facies is represented by one sample from the Valhall Formation, five samples from the Tuxen Formation, and one sample from the Sola Formation (Figs 5, A1(A–J); Table 2). The samples represent massive clay-bearing carbonate mudstone, consistent with homogenization by bioturbation. The concentration of pyrite crystals in one sample (Fig. A1(A)) probably reflects the location of a trace fossil, because these structures macroscopically are frequently seen to be rich in pyrite. Nannofossils (nannoconids) are seen to contain intrafossil porosity, but pore space is dominated by interparticle porosity with maximal pore diameter less than two microns. Angular pores in the mud matrix of samples represented in Figs A1(A) and A1(C) may be moulds. Calcite particles in samples represented in Figs 5 and A1(E–J) are contact-cemented, and especially the sample from the Valhall Formation (Fig. A1(I, J)) appears significantly recrystallized, causing the rare microfossils to appear as calcite aggregates.

Facies 3a. *Homogeneously bioturbated marly chalk*

This facies is represented by three samples from the Tuxen Formation (Figs 6, A1(K, L); Table 2). The microtexture is seen as a massive silicate-rich carbonate mudstone, where silicates dominate as supporting constituent. Uneven distribution of silicate particles gives rise to mottling on microscale and interparticle porosity with occasional pore diameter of more than two microns. Angular pores may be moulds. A calcitic aggregate represented in Fig. 6A may represent a recrystallized microfossil. This sample also contains disseminated crystals of pyrite (white).

Facies 4a. *Homogeneously bioturbated chalky marlstone*

This facies is represented by four samples from the Tuxen Formation (Figs 7A–D, A1(M–P); Table 2). The microtexture of these samples is a massive, clay-supported carbonate-rich mudstone, probably homogenized by bioturbation. Quartz and kaolinitic claystone clasts of silt size are noted in all samples. Pyrite aggregates, probably representing altered microfossils are relatively common in the sample represented in Fig. A1(O), which also contains shell fragments. Visible porosity is mainly intrafossil porosity, invisible interparticle porosity could reside in the pervasive clay matrix. Single crystals of calcite-rimmed dolomite are noted in Fig. 7A, C.

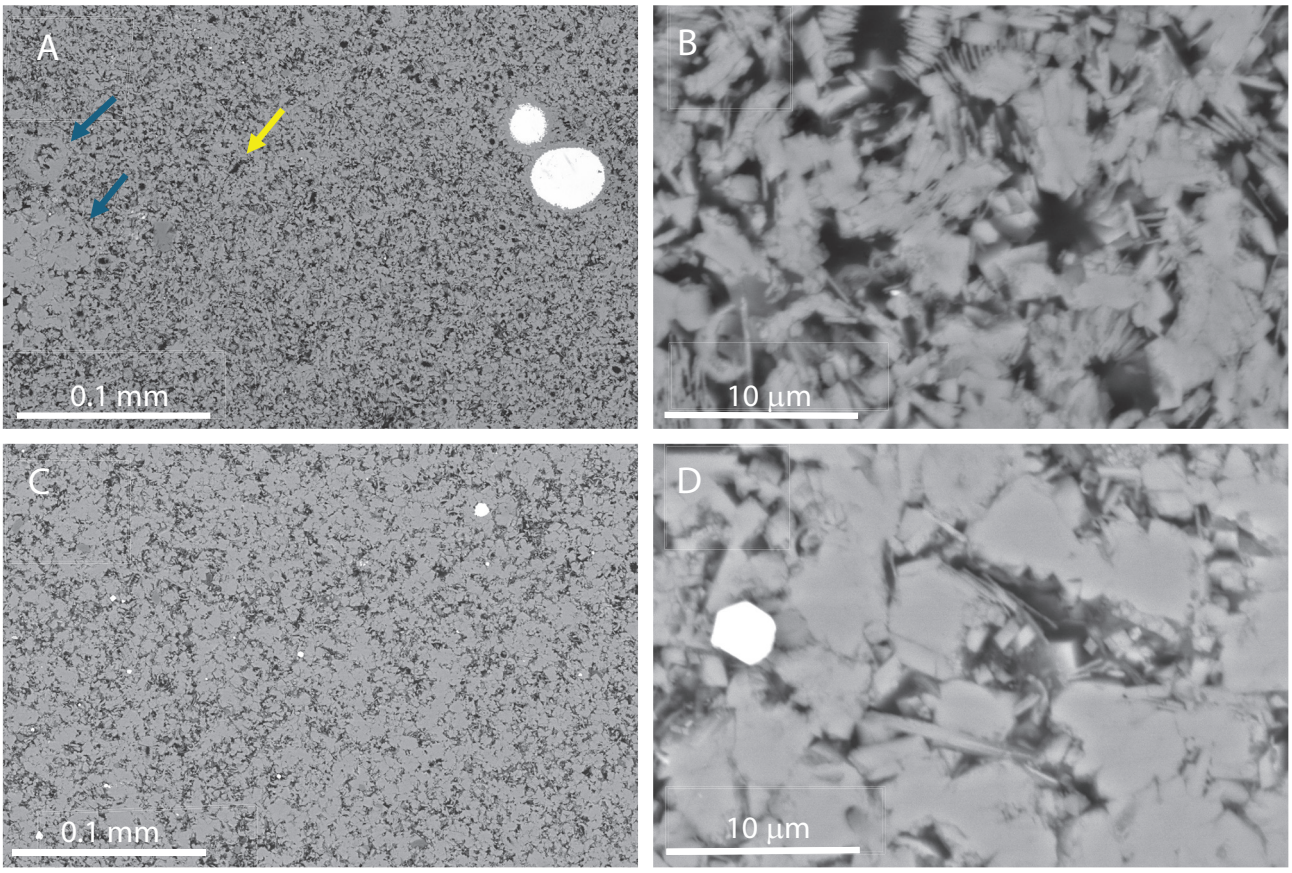


Fig. 4. Backscattered electron micrographs, illustrating texture (left) and pore geometry (right) of Facies 1a (homogeneously bioturbated chalk). (**A, B**) Sample from 8411'2'', Upper Tuxen Formation, oil zone (ref. Fig. 3). The mudstone texture illustrates partial recrystallization of carbonate mud and calcite cementation of calcareous microfossils (blue arrows). Some calcareous nannofossils have preserved intrafossil porosity (yellow arrow). A microfossil is cemented by pyrite (white). The closeup reveals the partial recrystallization of nannoconids, leaving partly degraded intrafossil porosity and high-specific surface crystallites of nannoconid skeletons with interparticle porosity. (**C, D**) Sample from 8478'3'', Middle Tuxen Formation, transition zone (ref. Fig. 3). Calcareous mudstone, where the presence of free water and sparsity of clay minerals may have facilitated the pronounced recrystallization of the carbonate mud. The white polygonal shape represents a pyrite crystal.

Facies 5a. *Homogeneously bioturbated marlstone*

This facies is represented by one sample from the Sola Formation (Fig. 7(E, F); Table 2). The sample represents a laminated, calcareous, clay-supported mudstone. Possible mouldic porosity, intrafossil porosity and interparticle porosity are seen. A plagioclase feldspar clast of 10 micron size is noted.

Facies 2b. *Biomottled slightly marly chalk*

This facies is represented by 11 samples from the Tuxen Formation and one sample from the Sola Formation (Figs 8, A2(A–T); Table 2). In most of these samples the microtexture is seen as massive clay-bearing carbonate mudstone, but in a few samples (Figs 8A, A2(E-P)) uneven distribution of calcitic and silicate particles results in visible mottling. Quartz silt particles are noted in several samples (Figs A2(G, J, L, R, T). Microfossils occur sparsely (Figs 8A, A2(C, G, M)) and are filled with calcite and minor pyrite cement. Nannofossils (nannoconids) are seen to contain intrafossil porosity, but pore space is dominated by interparticle porosity with maximal pore diameter less than two microns. Angular pores in the mud matrix of some samples (Figs 8A, A2(K, Q)) may be moulds. Calcite particles in all samples are contact-cemented. Pore-filling cement is noted in the deepest and stratigraphically lowest samples. Single crystals of calcite-rimmed dolomite are noted in sample represented in Fig. 8A, B.

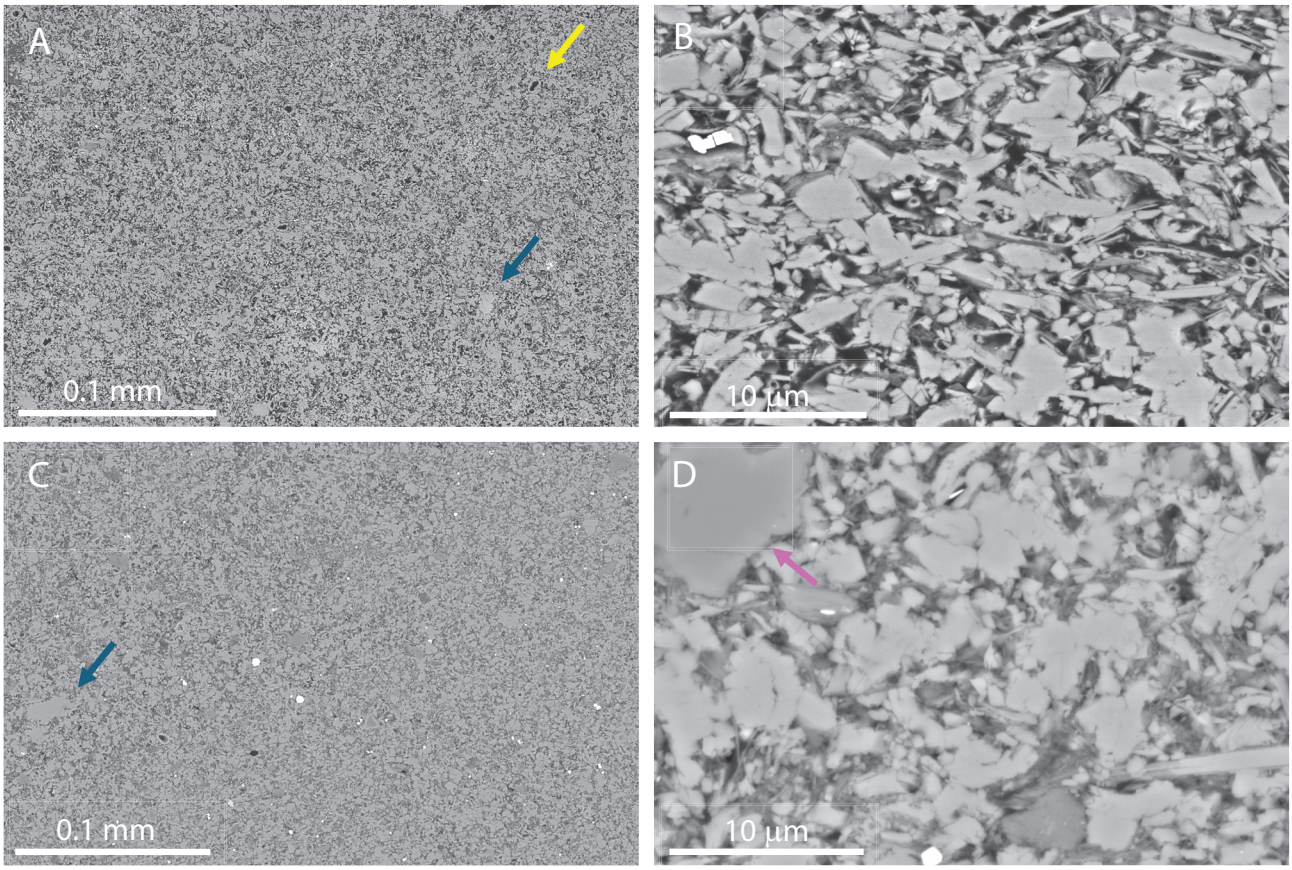


Fig. 5. Backscattered electron micrographs, illustrating texture (left) and pore geometry (right) of Facies 2a (homogeneously bioturbated slightly marly chalk). (**A, B**) Sample from 8456'11'', Middle Tuxen Formation, upper part of transition zone (ref. Fig. 3). The sample has a massive mudstone texture with single calcareous nannofossils, some with preserved intrafossil porosity (yellow arrow), and some cemented by calcite (blue arrow). The closeup reveals local lamination of clay particles (medium grey) and partly recrystallized calcareous nannofossils (light grey) leaving a homogeneous pore space with high specific surface of the interparticle porosity. (**C**, **D**) Sample from 8586', Lower Tuxen Formation, lower part of transition zone (ref. Fig. 3). The sample has massive mudstone texture with single calcareous microfossils cemented by calcite (blue arrow) and submicron-sized pyrite crystals (white). The closeup highlights quartz silt (pink arrow) and clay particles mixed with recrystallized calcite particles of altered biogenic shape. Interparticle porosity is only partly visible at the chosen magnification

Facies 3b. *Biomottled marly chalk*

This facies is represented by eight samples from the Tuxen Formation and one sample from the Sola Formation (Figs 9, A2(U–HH); Table 2). In most of these samples the microtexture is a mottled, clay-bearing carbonate mudstone, where mottling is caused by an uneven distribution of calcitic and silicate particles. Samples generally appear massive. Silt particles of quartz and kaolinitic claystone are noted in samples represented in Figs 9A and A2(BB, DD). Microfossils occur sparsely (Fig. A2(Y, AA, CC)), whereas shell fragments are seen in Figs 9A and A2(CC). Microfossils are filled with calcite or pyrite cement. Nannofossils (nannoconids) are seen to contain intrafossil porosity (Figs 9D and A2(V, X, Z)) but pore space is dominated by interparticle porosity with maximal pore diameter less than two microns. Angular pores in the mud matrix of samples represented in Figs 9A and A2(U, Y, CC) may be moulds. Calcite particles in deeper samples are contact-cemented (Figs 9D, A2(BB, FF, HH)). In these deeper samples, clay minerals seem to form discrete aggregates, whereas clay minerals in upper samples (Figs 9B and A2(V, X, Z)) form a pore-filling network among calcite particles.

Facies 4b. *Biomottled chalky marlstone*

This facies is represented by one sample from the Valhall Formation, one sample from the Tuxen Formation, and one sample from the Sola Formation (Figs 10, A2(II, JJ); Table 2). The microtexture of these samples is a laminated, clay-supported, carbonate-rich mudstone. Rounded pores may represent moul-

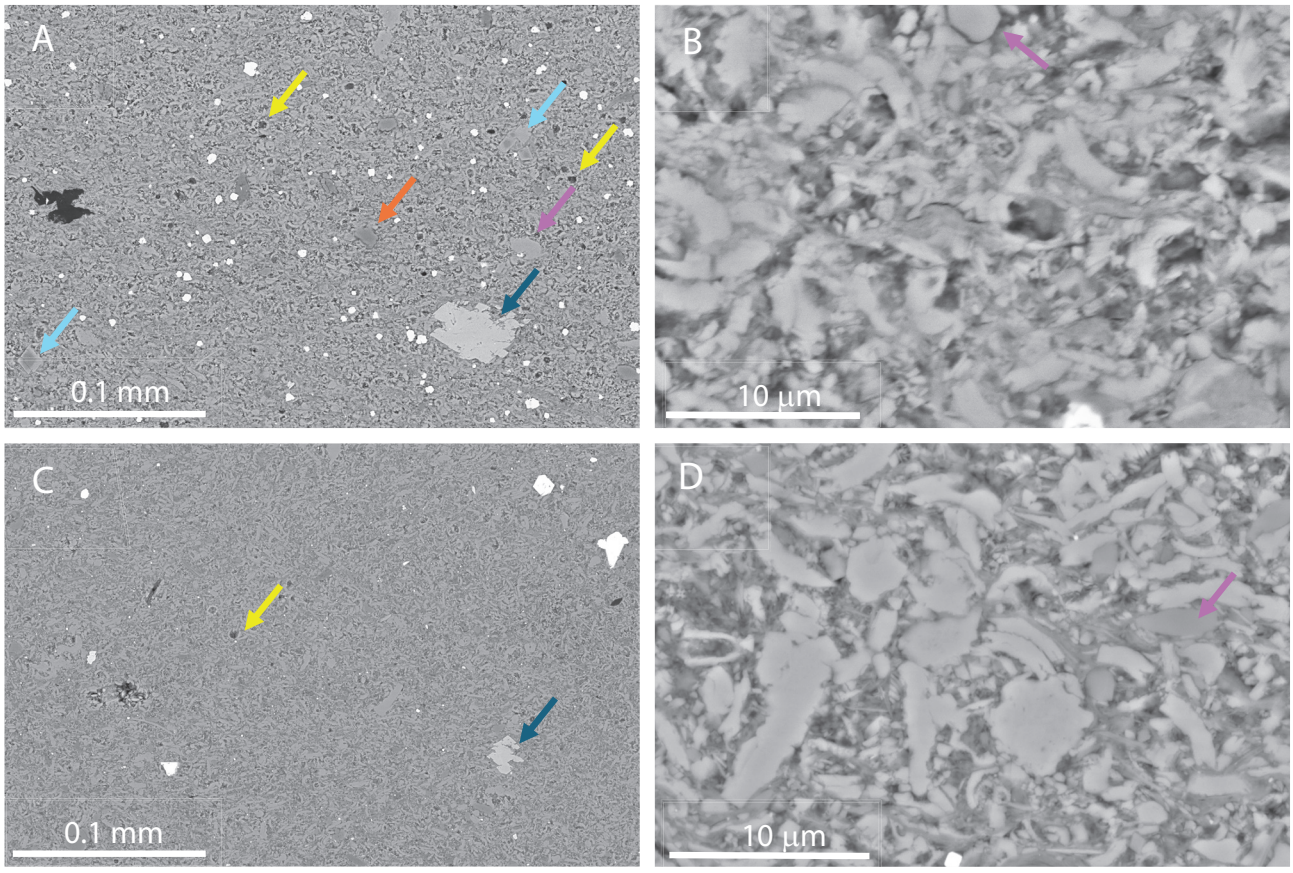


Fig. 6. Backscattered electron micrographs, illustrating texture (left) and pore geometry (right) of Facies 3a (homogeneously bioturbated marly chalk). (**A, B**) Sample from 8536′, Lower Tuxen Formation. (**C**, **D**) Sample from 8579′, Lower Tuxen Formation. Both samples are from lower part of the transition zone (ref. Fig. 3). The samples have massive mudstone texture with single calcitic aggregates probably representing recrystallized microfossils (blue arrows) and single calcareous nannofossils, some with preserved intrafossil porosity (yellow arrows). Silt particles include quartz (pink arrow) and in sample from 8536′ (**A**) also kaolinitic claystone clasts (orange arrow). This sample (**A**) contains calcite-coated dolomite crystals (light blue arrows) and submicron-sized pyrite crystals (white). The sample from 8579′ (**C**) contains micron-sized pyrite crystals. The closeups highlight dense mixtures of quartz silt (pink arrows), clay particles and recrystallized calcite particles of altered biogenic shape. Interparticle porosity is only partly visible at the chosen magnification.

dic porosity, and only little interparticle porosity is visible. The sample represented in Fig. 10A, B contains disseminated micron-sized pyrite crystals. In sample represented in Fig. 10C, D, pyrite is localized in larger aggregates/crystals.

Facies 5b. *Biomottled marlstone*

This facies is represented by one sample from the Tuxen Formation and one sample from the Sola Formation (Fig. 11; Table 2). The samples represent a massive, clay-rich, calcareous mudstone texture in which calcite- and silicate particles are unevenly distributed, giving rise to a mottled appearance. Intrafossil, possible mouldic and interparticle porosity are seen in areas rich in calcite. The sample represented in Fig. 11A, B contains scattered pyrite crystals up to five microns in size.

Facies 4c. *Parallel-laminated chalky marlstone*

This facies is represented by one sample from the Sola Formation (Fig. 12A, B; Table 2). The microtexture is a laminated, calcareous, clay-supported mudstone. Interparticle porosity is visible in laminae rich in calcitic particles, intrafossil porosity and micron-size questionable moulds are relatively common. Micron-sized pyrite occurs as single crystals and loose aggregates. Quartz silt particles of 10 micron size are noted.

Facies 5c. *Parallel-laminated marlstone*

This facies is represented by seven samples from the Tuxen Formation, of which six samples are from the Munk Marl Bed and two samples from the Sola For-

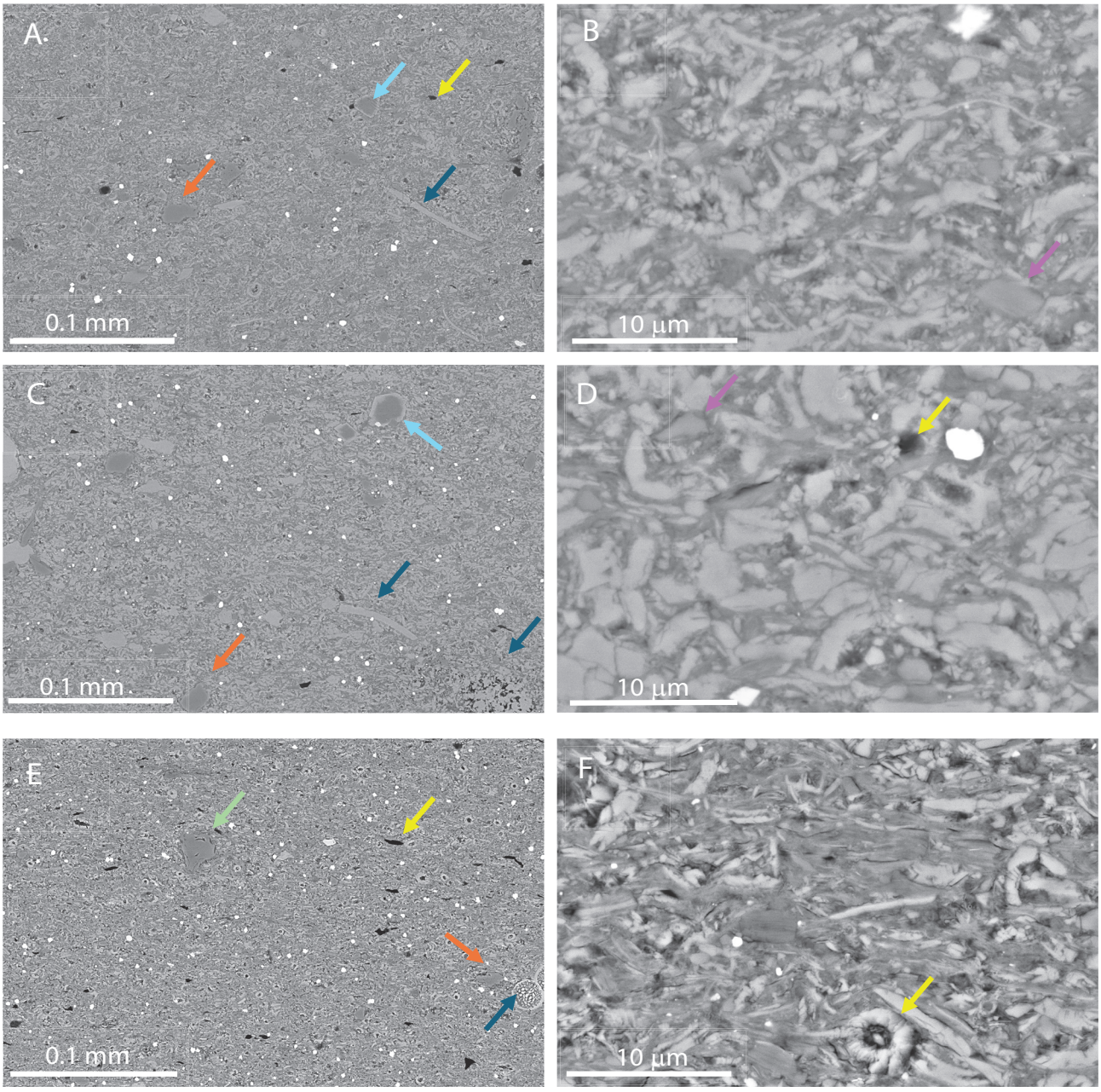


Fig. 7. Backscattered electron micrographs, illustrating texture (left) and pore geometry (right) of Facies 4a (homogeneously bioturbated chalky marlstone; **A–D**) and Facies 5a (homogeneously bioturbated marlstone; **E–F**). (**A**, **B**) Sample from 8532'4'', Lower Tuxen Formation. (**C**, **D**) Sample from 8582'4'', Lower Tuxen Formation. Both samples are from lower part of the transition zone (ref. Fig. 3). The samples have massive mudstone texture with single calcareous fossil clasts and partly recrystallized calcareous microfossils (blue arrows). Silt particles include quartz (pink arrows) and kaolinitic claystone clasts (orange arrows). Both samples contain calcite-coated dolomite crystals (light blue arrows) and submicron-sized pyrite crystals (white). The closeups highlight dense mixtures of quartz silt (pink arrows), clay particles and partly recrystallized biogenic calcite particles. Up to micron-sized porosity may in some cases represent moulds, in other cases shelter porosity (yellow arrow). Interparticle porosity is not visible at the chosen magnification. (**E**, **F**) Sample from 8381'11'', Lower Sola Formation. The sample is from the oil zone (ref. Fig. 3). The sample has mudstone texture with slight lamination indicated by orientation of fossil clasts and voids. A calcareous microfossil has intrafossil porosity (blue arrow). Silt particles include feldspar (green arrow) and kaolinitic claystone clasts (orange arrow). Submicron-sized pyrite crystals are widespread (white). The closeup highlights the dense mixture of clay particles and nannofossil debris. Up to micron-sized pin point porosity may in some cases represent moulds, in other cases intrafossil porosity (yellow arrow).

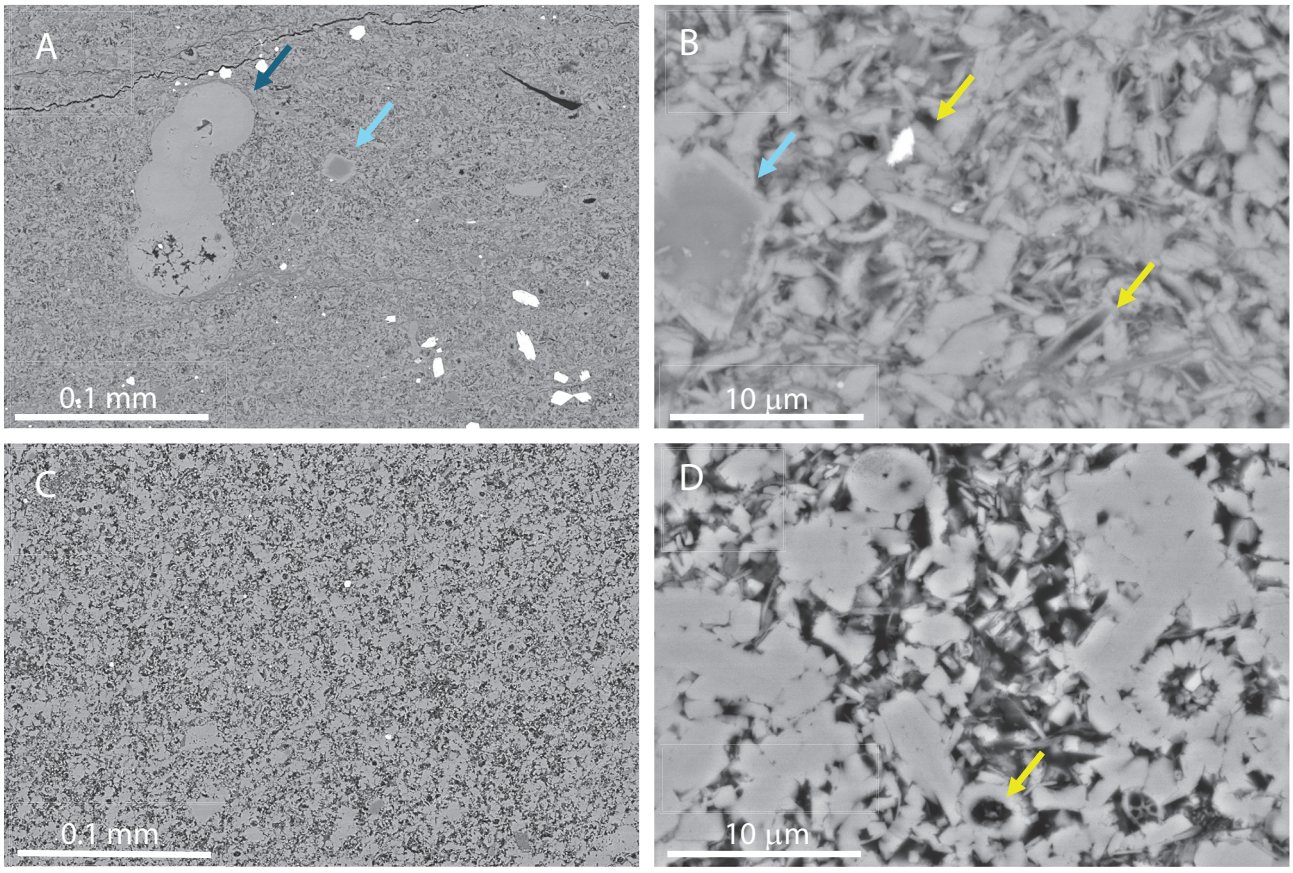


Fig. 8. Backscattered electron micrographs, illustrating texture (left) and pore geometry (right) of Facies 2b (biomottled slightly marly chalk). (**A, B**) Sample from 8430'11'', Middle Tuxen Formation, the oil zone (ref. Fig. 3). The sample has mudstone texture with a foraminifer almost completely cemented by ferroan calcite (blue arrow). Mottling is revealed by uneven distribution of visible interparticle porosity at low magnification. The sample contains calcite-coated dolomite crystals (light blue arrows) and micron-sized pyrite crystals (white). The closeup highlights partly recrystallized nannofossil debris, local lamination in clay content, interparticle porosity and intrafossil porosity (yellow arrows). (**C**, **D**) Sample from 8574'1'', Lower Tuxen Formation, lower part of transition zone (ref. Fig. 3). Calcareous mudstone, where the presence of free water and sparsity of clay minerals have probably facilitated the pronounced recrystallization of the carbonate mud. The closeup reveals recrystallized nannofossils where intrafossil porosity is preserved (yellow arrow). The relatively regular neomorphic calcite and remains of fossils give rise to a moderate specific surface of the interparticle porosity.

mation (Figs 12C–F, A3; Table 2). All samples have laminated, calcite-bearing, silicate mudstone texture. Silt size particles are noticed in samples represented in Fig. A3(J, L). Porosity is visible in most samples but could reflect sample desiccation prior to impregnation with epoxy resin. In most of the samples from the Munk Marl Bed, lamination seems to have been disturbed by shear deformation (Fig. A3(G, K, M)). All samples contain pyrite as micron-sized crystals or in a single sample (Fig. A3(H)) as framboids.

Facies 2x. *Flaser-laminated slightly marly chalk*

This facies is represented by one sample from the Tuxen Formation (Fig. 13; Table 2). The sample is a carbonate-rich, silicate-supported mudstone. The macroscopically described flaser lamination (Jelby *et al.* 2022) is microscopically reflected in uneven laminae of calcite particles and silicates in possible deformation (compaction) bands. The pore space is dominated by interparticle porosity with maximal pore diameter less than two microns. Angular pores in mud matrix may be moulds.

Facies 2y. *Shear-deformed slightly marly chalk*

This facies is represented by five samples from the Tuxen Formation (Figs 14A, B, A4); Table 2). All samples have massive clay-bearing carbonate mudstone texture. Quartz silt is noted (Fig. A4(B, H)). Pore space is dominated by interparticle porosity with maximal pore diameter less than two microns. Calcite particles in all samples are contact-cemented. Single crystals of calcite-rimmed dolomite are pres-

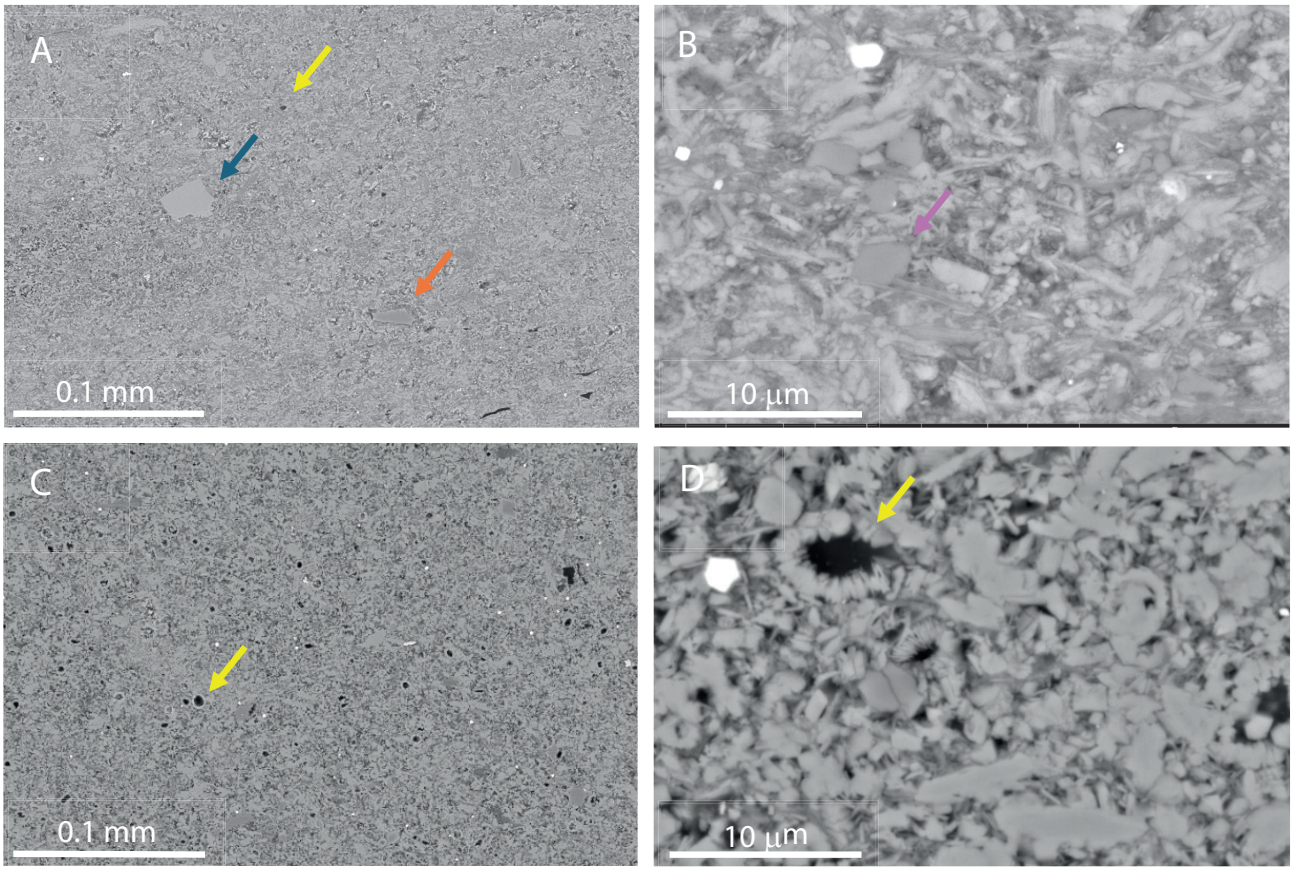


Fig. 9. Backscattered electron micrographs, illustrating texture (left) and pore geometry (right) of Facies 3b (biomottled marly chalk). (**A, B**) Sample from 8369'11'', Lower Sola Formation, the oil zone (ref. Fig. 3). The sample has mudstone texture, where mottling is revealed by uneven distribution of visible interparticle porosity at low magnification. A single fossil fragment is seen (blue arrow), as well as a claystone clast (orange arrow). Possibly mouldic porosity is seen (yellow arrow). Closeup reveals mixture of nannofossil debris, quartz silt (pink arrow) and clay, as well as single submicron-sized pyrite crystals (white). Interparticle porosity is partly visible at the chosen magnification. (**C**, **D**) Sample from 8568'8'', Lower Tuxen Formation, lower part of the transition zone (ref. Fig. 3). The sample has mudstone texture with a less pronounced mottling of interparticle porosity at low magnification than the oil zone sample. Closeup reveals partly recrystallized nannofossil debris as well as single submicron-sized pyrite crystals (white). Interparticle porosity is well visible and has moderate specific surface. Intrafossil porosity in nannoconids is visible at both magnifications (yellow arrows).

ent (Fig. A4(G, H)). The shear deformation structures observed macroscopically are not visible in these electron microscope images.

Facies 3y. *Shear-deformed marly chalk*

This facies is represented by one sample from the Tuxen Formation (Fig. 14C, D; Table 2). The sample has a massive, clay-bearing carbonate mudstone texture. Calcite particles are contact-cemented and pore-filling cement is found as disseminated less than 10 micron-sized aggregates. Nannofossils (nannoconids) are seen to contain intrafossil porosity, but pore space is dominated by interparticle porosity with maximal pore diameter less than two microns. The macroscopically observed shear deformation structures are not visible in this electron microscope image.

Facies 4y. *Shear-deformed chalky marlstone*

This facies is represented by one sample from the Sola Formation (Fig. 14E, F; Table 2). This sample represents a massive, clay-bearing, calcareous mudstone with well-preserved remains of nannofossils. Intrafossil porosity and more dominating interparticle porosity are clearly visible. Macroscopically observed shear deformation structures are not obvious from these electron microscope images.

Facies 5y. *Shear-deformed marlstone*

This facies is represented by one sample from the Sola Formation (Fig. 14G, H; Table 2). It has a massive, clay-supported, calcite-rich mudstone texture. Visible porosity is mainly intrafossil porosity in nan-

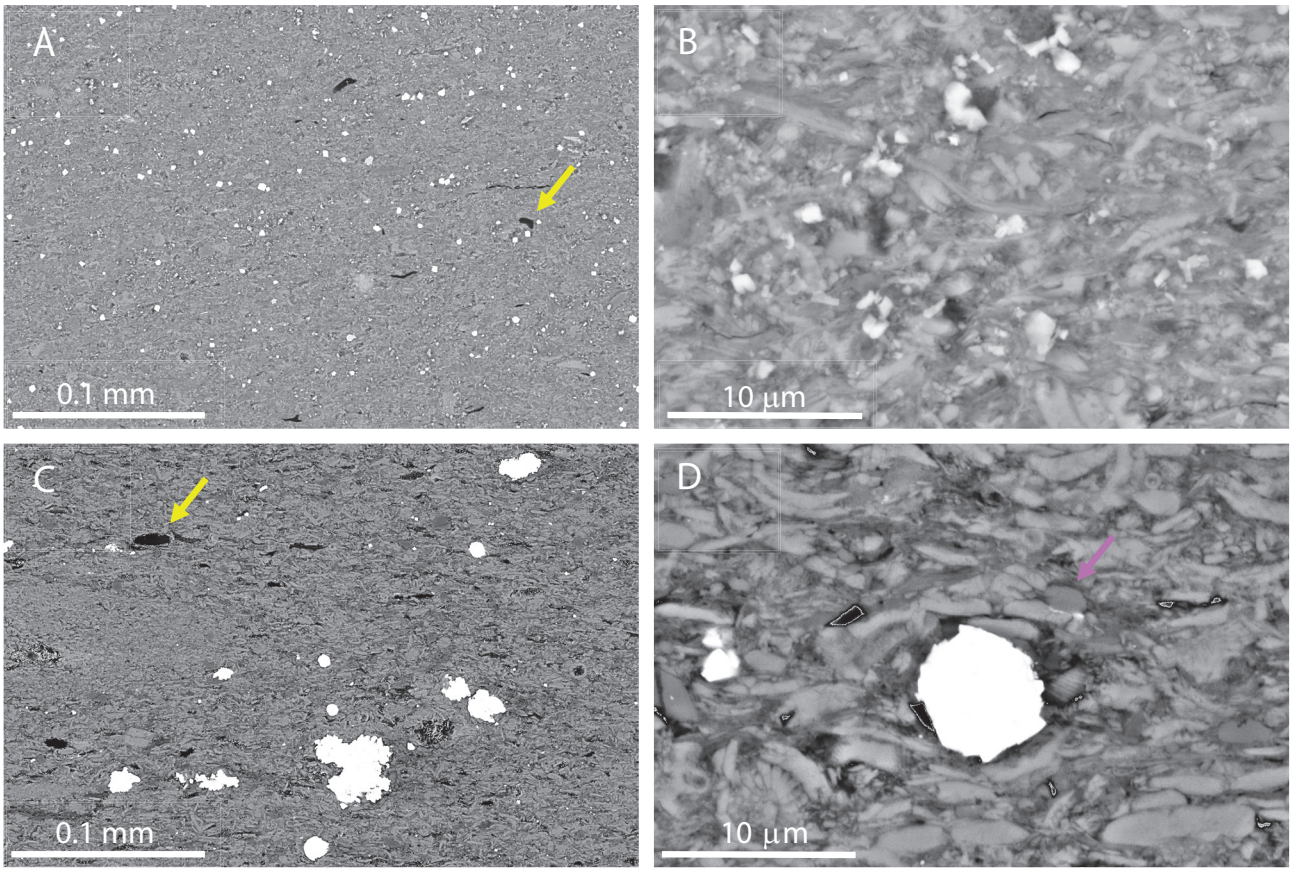


Fig. 10. Backscattered electron micrographs, illustrating texture (left) and pore geometry (right) of Facies 4b (biomottled chalky marlstone). (**A, B**) Sample from 8369'1'', Middle Sola Formation, the oil zone (ref. Fig. 3). The sample has mudstone texture with faint lamination as indicated by nannofossil fragments and possible moulds (yellow arrow). The closeup reveals a dense mixture of nannofossil debris and clay with scattered submicron size pyrite crystals (white). Interparticle porosity is locally visible. (**C**, **D**) Sample from 8491'1'', Lower Tuxen Formation, upper part of the transition zone (ref. Fig. 3). The sample has mudstone texture with pronounced mottling as revealed by the distribution of interparticle porosity. It also has some horizontal lamination as indicated by orientation of voids, possibly representing moulds (yellow arrow). Pyrite crystals of up to 40 micron size (white) are seen. The closeup reveals a laminated mixture of nannofossil debris, clay and quartz silt (pink arrow) with some visible interparticle porosity.

noconids. Micron-sized pyrite crystals are disseminated in the sample. Macroscopic shear deformation structures are not observed at electron microscope scale.

Facies 2z. *Silicified slightly marly chalk*

This facies is represented by two samples from the Tuxen Formation and one sample from the Sola Formation (Figs 15A, B, A5; Table 2). The microtexture of the two deeper samples (Fig. A5) is seen as massive clay-bearing carbonate mudstone, whereas the upper sample is seen as an unevenly silica-cemented, clay-bearing carbonate mudstone (Fig. 15A, B). Calcite-cemented microfossils occur sparsely (Fig. A5(C)). Pore space is dominated by interparticle porosity with maximal pore diameter less than two microns but appears heterogeneously distributed in the silica-cemented sample (Fig. 15A, B). Calcite particles in samples from the Tuxen Formation are contact-cemented (Fig. A5(B, D)). Possible incipient silica cement is noted in pore space of these samples.

Facies 3z. *Silicified marly chalk*

This facies is represented by one sample from the Tuxen Formation (Fig. 15C, D; Table 2). It has a massive, silicate-bearing carbonate mudstone texture. Calcite particles are contact-cemented and pore-filling silica cement is disseminated leaving local interparticle porosity open. Micron-sized pyrite crystals are disseminated in the sample.

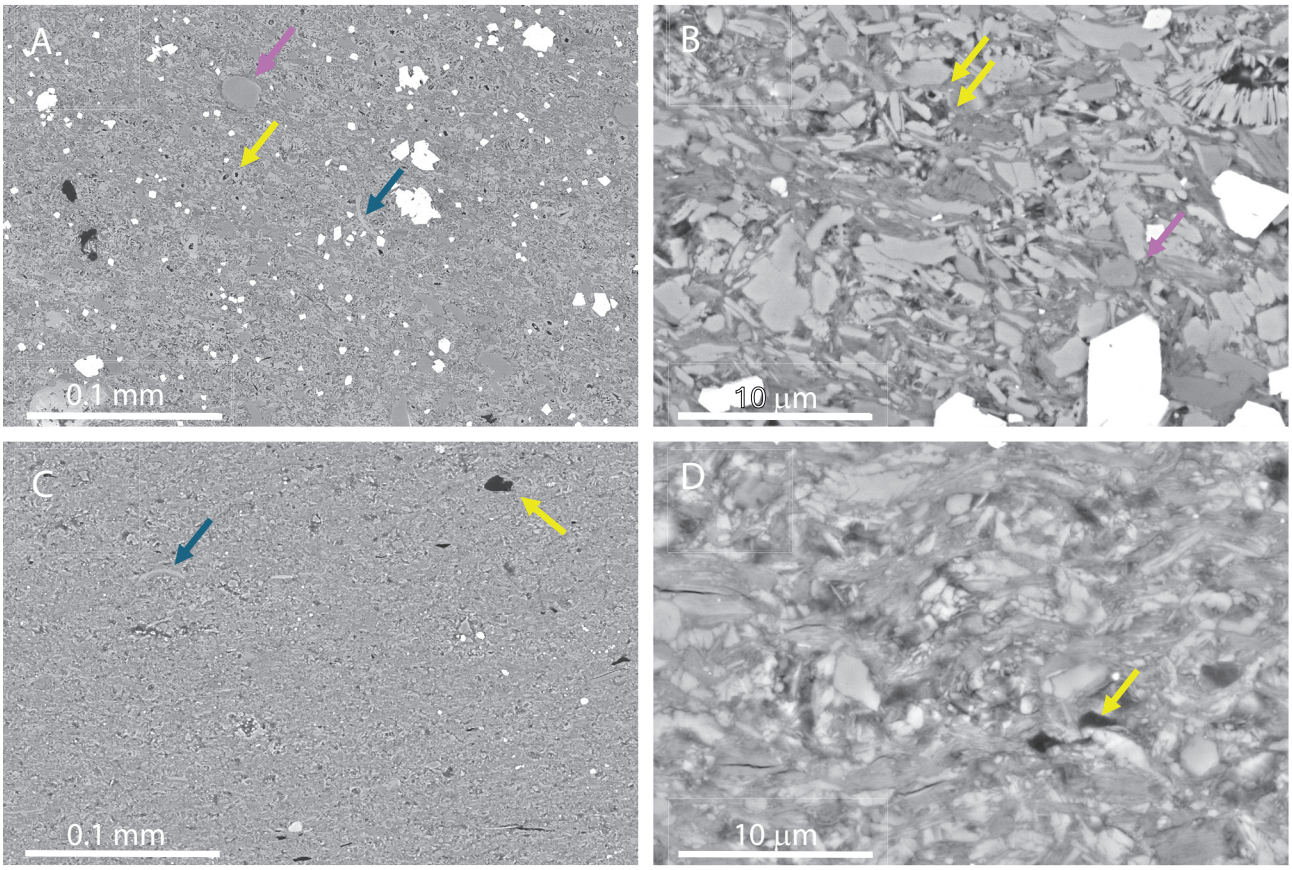
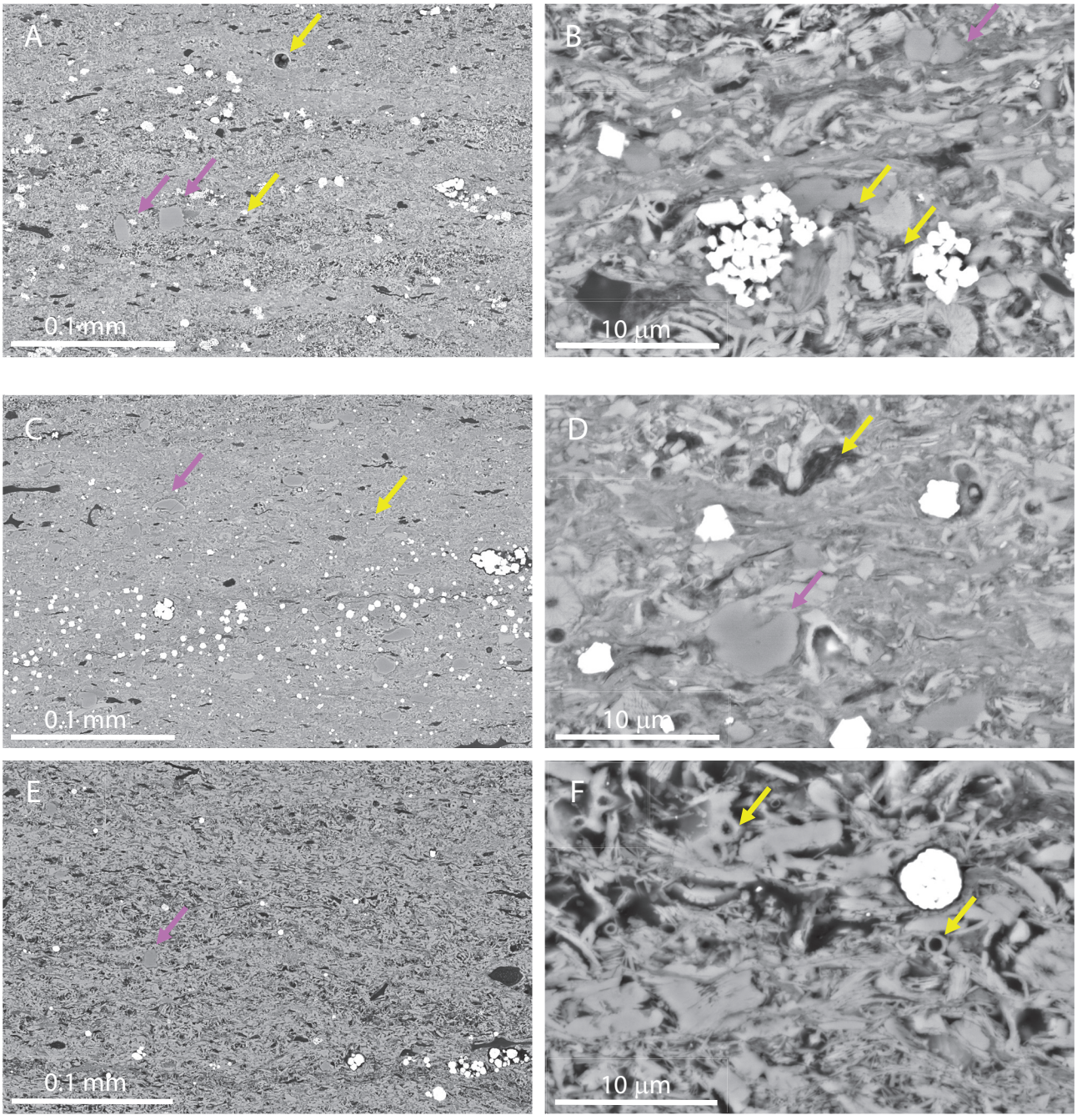


Fig. 11. Backscattered electron micrographs, illustrating texture (left) and pore geometry (right) of Facies 5b (biomottled marlstone). (**A, B**) Sample from 8388'4'', Lower Sola Formation, oil zone (ref. Fig. 3). The sample has massive mudstone texture with single microfossil clasts (blue arrow) and grains of quartz silt (pink arrow), as well as scattered up to 10 micron-sized pyrite crystals (white). Intra-nannofossil porosity is widespread (yellow arrow). The closeup reveals a dense mixture of partly recrystallized nannofossil debris and clay with quartz silt and scattered pyrite crystals (white). Interparticle porosity is locally visible (yellow arrow). (**C, D**) Sample from 8416', Middle Tuxen Formation, upper part of transition zone (ref. Fig. 3). The sample has massive mudstone texture with single microfossil clasts (blue arrow) and scattered less than micron size pyrite crystals (white). Possible mouldic porosity is locally visible (yellow arrow). The closeup reveals a dense mixture of clay and micron size calcitic debris. Interparticle porosity is locally visible (yellow arrow).

Fig. 12. Backscattered electron micrographs, illustrating texture (left) and pore geometry (right) of Facies 4c (parallel-laminated chalky marlstone; **A, B**) and Facies 5c (parallel-laminated marlstone; **C–F**). (**A**, **B**) Sample from 8352'1'', Middle Sola Formation, oil zone (ref. Fig. 3). The sample has mudstone texture with lamination caused by variation in clay content. It contains quartz silt (pink arrow) and nannofossils. Submicron size pyrite crystals (white) occur in both clay-rich and clay-poor intervals. Mouldic porosity is widespread together with rarer intrafossil porosity (yellow arrow). The closeup reveals nannofossil debris in layers with dense packing with clay and quartz silt (pink arrow) alternating with layers with interparticle porosity (yellow arrow). Submicron size pyrite in framboidal aggregate is seen (white). (**C**, **D**) Sample from 8348'4'', Middle Sola Formation, oil zone (ref. Fig. 3). The sample has mudstone texture with lamination caused by variation in clay content. It contains quartz silt (pink arrow). Submicron-sized pyrite crystals (white) occur primarily in clay-poor intervals. Mouldic porosity is widespread together with rarer intrafossil or shelter porosity (yellow arrow). The closeup reveals nannofossil debris in layers with dense packing with clay and quartz silt (pink arrow) alternating with layers with interparticle porosity (yellow arrow). Submicron size pyrite is seen (white). (**E**, **F**) Sample from 8488'11'', Munk Marl Bed in the transition zone (ref. Fig. 3). The sample has mudstone texture with lamination caused by variation in clay content. It contains quartz silt (pink arrow). Submicron size pyrite crystals (white) occur locally. Mouldic and interparticle porosity are widespread. The closeup reveals nannofossil debris in layers with loose packing with clay alternating with layers with interparticle porosity and local intra nannofossil porosity (yellow arrows). Micron size pyrite is seen (white).



Discussion: Origin of microscopic features

Microscopic depositional features versus macroscopic facies

Microscopic features deemed to represent sedimentary processes or diagenesis are listed in Table 3. With respect to depositional features, all studied samples have carbonate mudstone texture, where the supporting mineral is calcite in most samples. Clay-supported texture is rare and mainly confined to chalky marlstone and marlstone (Fig. 7). Biogenic calcareous components represent pelagic organisms (mainly nannofossils such as nannoconids; e.g. Fig. 14) and debris. Pelagic foraminifers are sparsely represented (Figs 4, 8), and benthic biofragments are virtually absent. The scarcity of benthos in the Lower Cretaceous chalks was noted by Jelby *et al.* (2022) and Lauridsen *et al.* (2022); the latter authors suggested that sea-floors consisting of pelagic carbonate ooze had not existed in the study area before the Early Cretaceous and that benthic organisms had yet to

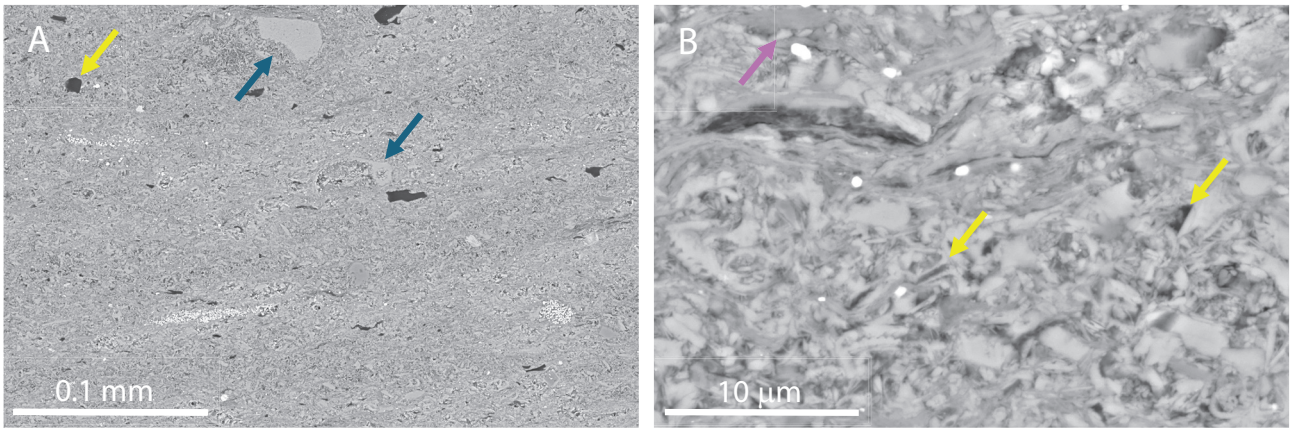


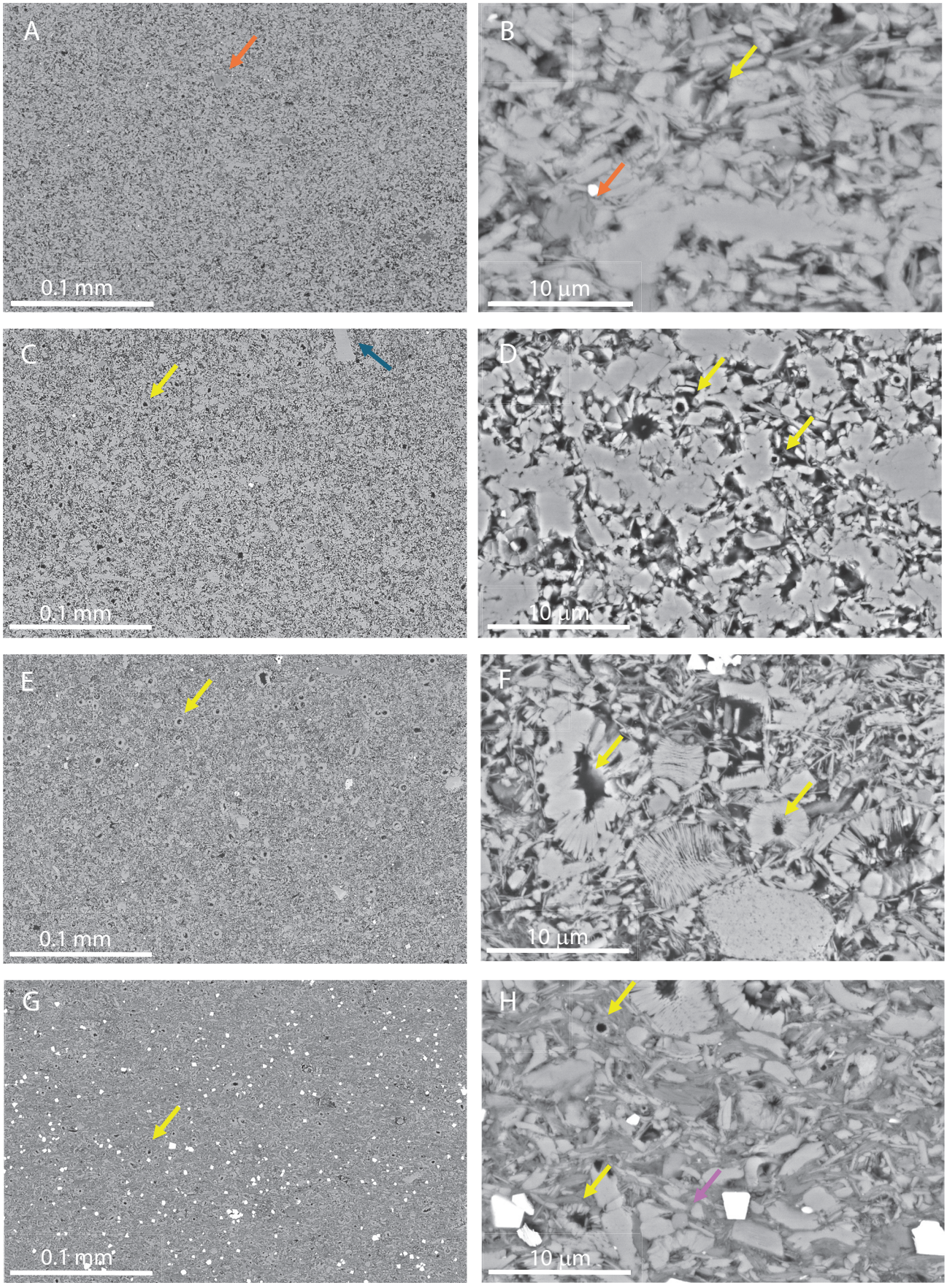
Fig. 13. Backscattered electron micrographs illustrating texture (left) and pore geometry (right) of Facies 2x (flaser-laminated slightly marly chalk). (**A, B**) 8444'11'', Middle Tuxen Formation. The sample is from upper part of the transition zone (ref. Fig. 3) and has mudstone texture. It has contorted lamination representing varying clay content. Fossil debris (blue arrows) and mouldic porosity (yellow arrow) occur locally. Clusters of submicron size pyrite (white) are seen. The closeup reveals nannofossil debris locally packed with clay and quartz silt (pink arrow) and locally bearing interparticle porosity and even intra-nannofossil porosity (yellow arrows).

adapt to the substrate. This model, however, does not explain the scarcity of planktonic microfossils. Biogenic debris is mainly composed of calcite. Silt particles of quartz (Fig. 5) and kaolinitic claystone occur throughout the slightly marly chalk to marlstone lithologies (Fig. 7; Table 3), and a single silt-sized clast of plagioclase feldspar was noted in a marlstone from the lower Sola Formation (8381'11'') (Fig. 7). The clay component is predominately detrital and is primarily kaolinite. The relatively frequent occurrence of kaolinitic claystone clasts points to a nearby source of detrital sediments in accordance with Blok *et al.* (2022, 2023). The dominance of kaolinite and quartz silt together with clay-sized kaolinite point to a weathered granitic source and possible transport by mass flow. The Munk Marl Bed has been reported to have a high concentration of organic matter (Jensen & Buchardt 1987), but this was not unequivocally identified from the SEM sample inspection. Organic particles may be difficult to distinguish from impregnated pores, and resultingly they may have been overlooked.

The macroscopically homogeneous bioturbation appears massive in thin section, although biomottling and trace fossils mainly are discernible in the more clay-rich marlstone lithologies (marly chalk, chalky marlstone and marlstone) (Figs 9, 11). The fact that biomottling is identifiable in the BSE micrographs indicates that the uneven distribution of non-carbonate particles, and thus bioturbation, also occurs at the microscopic scale (Fig. 6).

The macroscopically parallel-laminated Facies 4c and 5c, also microscopically appear laminated and represent the clay-rich chalky marlstone and marlstone lithologies. Shear-deformation has previously been argued as having a significant influence on microfabric based on analyses of porosity patterns in the Upper Cretaceous Chalk Group (Anderskouv & Surlyk 2012), and indeed localized pore collapse caused by stress with a shear component has been

Fig. 14. Backscattered electron micrographs illustrating texture (left) and pore geometry (right) of Facies 2y (shear-deformed slightly marly chalk; **A, B**), Facies 3y (shear-deformed marly chalk; **C**, **D**), Facies 4y (shear-deformed chalky marlstone; **E**, **F**) and Facies 5y (shear-deformed marlstone; **G**, **H**). (**A, B**) Sample from 8413'1'', Middle Tuxen Formation, upper part of transition zone (ref. Fig. 3). The sample has massive mudstone texture with single kaolinitic claystone clasts (orange arrow). The closeup reveals densely packed partly recrystallized nannofossil debris and widespread interparticle porosity (yellow arrow). (**C**, **D**) Sample from 8526'11'', Lower Tuxen Formation. The sample is from the transition zone (ref. Fig. 3) and has massive mudstone texture with single fossil fragments (blue arrow). Intra-microfossil porosity is widespread (yellow arrow). The closeup reveals recrystallized but still visibly biogenic nannofossils with some preserved intrafossil porosity and widespread interparticle porosity (yellow arrows). (**E**, **F**) Sample from 8350'5'', Middle Sola Formation, oil zone (ref. Fig. 3). The sample has massive mudstone texture. Intrafossil porosity is widespread (yellow arrow). The closeup reveals nannofossil debris (including nannoconids) with minor clay. Intrafossil (yellow arrows) and interparticle porosity are widespread. (**G**, **H**) Sample from 8385'11'', Lower Sola Formation, oil zone (ref. Fig. 3). The sample has massive mudstone texture. Intrafossil porosity is widespread (yellow arrow) as are submicron-sized pyrite crystals (white). The closeup reveals partly recrystallized nannofossil debris (including nannoconids) packed with clay and quartz silt (pink arrow). Micron size pyrite crystals (white) are seen. Intrafossil porosity (yellow arrows) and local interparticle porosity are noted.


A
0.1 mm
B
10 µm
C
0.1 mm
D
10 µm
E
0.1 mm
F
10 µm
G
0.1 mm
H
10 µm

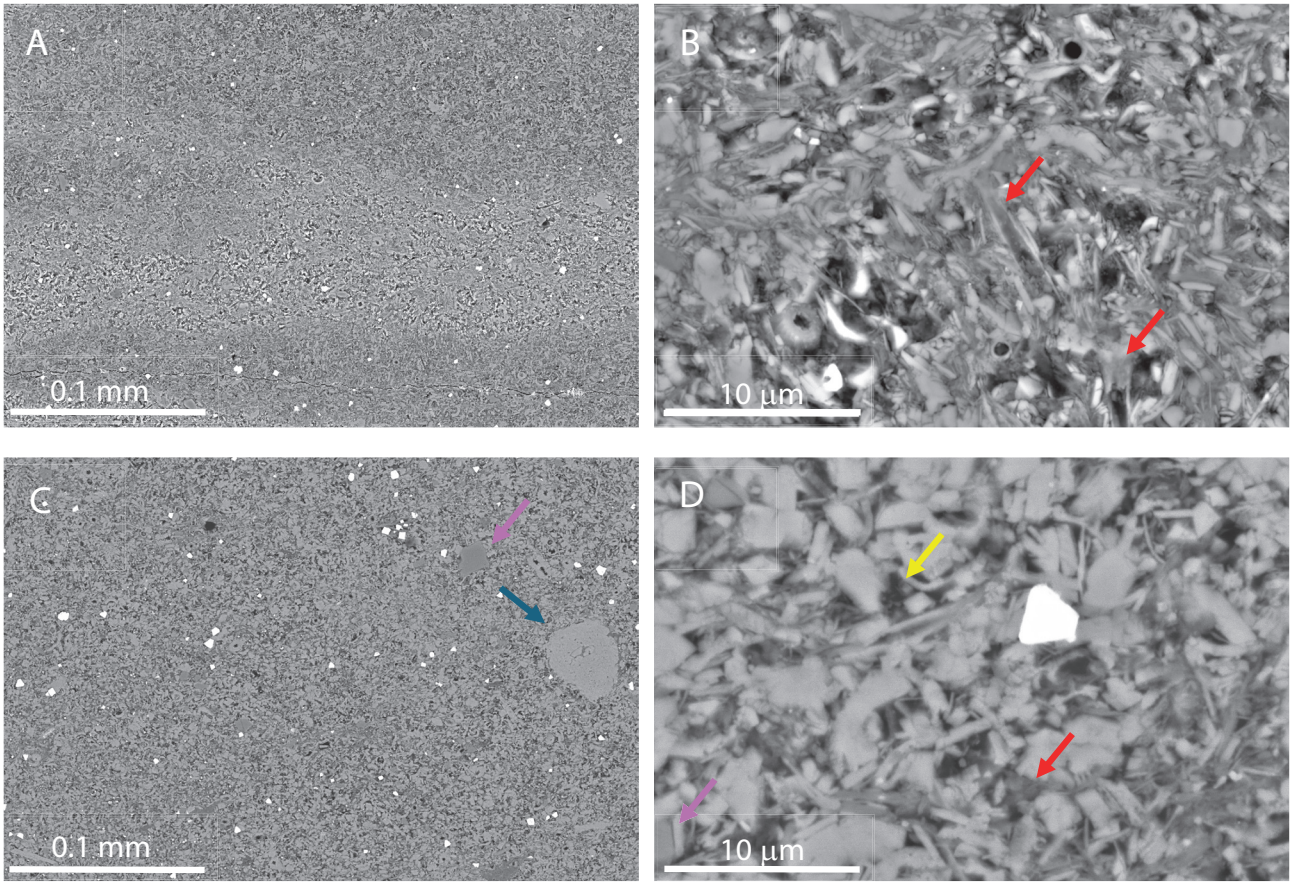


Fig. 15. Backscattered electron micrographs, illustrating texture (left) and pore geometry (right) of Facies 2z (silicified slightly marly chalk; **A, B**) and Facies 3z (silicified marly chalk; **C**, **D**). (**A**, **B**) Sample from 8377'2", Lower Sola Formation, oil zone (ref. Fig. 3). The sample has massive mudstone texture and is unevenly cemented by silica (red arrow). (**C**, **D**) Sample from 8495'1", Lower Tuxen Formation. The sample is from the transition zone (ref. Fig. 3) and has massive mudstone texture with single bioclasts (blue arrow) and quartz silt (pink arrow). Submicron size pyrite crystals (white) are widespread. The closeup reveals moderately recrystallized nannofossil debris, loosely packed with clay and quartz silt (pink arrow). Local possible silica cement is indicated with red arrow. The sample holds widespread interparticle porosity (yellow arrow).

found to result in deformation bands (Wennberg *et al.* 2013; Fabricius 2020). Macroscopically observed deformation bands (Jelby *et al.* 2022) were not observed microscopically, perhaps due to not being sampled (Figs 14, A4).

Shallow burial diagenesis

Pyrite is abundant, generally as dispersed submicron-sized crystals, especially in the more clay-rich facies (Fig. 6). In some cases, the pyrite is localized in layers or clusters, probably reflecting trace fossils (Fig. A1(A)), and in one instance as framboids (in the Munk Marl Bed; Fig. A3(H)). Pyrite in pelagic carbonate ooze has been shown to form at shallow depth when organic matter is consumed by sulphate-reducing bacteria and substituted by pyrite. Musgrave *et al.* (1993) demonstrated how this process can lead to dissolution of magnetite, because Fe is needed for the precipitation of pyrite.

Dolomite is locally present as single crystals (Figs 6–8). The diagenetic formation of this mineral requires a source of magnesium. A typical source would be biogenic, e.g. high-magnesium calcite dissolved during early recrystallization at shallow burial (e.g. Eberli *et al.* 1997). All observed dolomite crystals are overgrown by calcite.

The clay-poor intervals contain minute unidentifiable calcitic particles, which for simplicity is described as nannofossil debris (Figs 4, 5), although an abiogenic diagenetic origin cannot be fully precluded (Tagliavento *et al.* 2021).

Burial diagenesis – impact of oil saturation

Nannofossils are in different degrees of recrystallization, reflecting oil saturation and clay content. The best preserved nannofossils are found in the oil zone,

Table 3. Overview of microscopic observations

Stratigraphy	Lithology and facies	Depositional features	Diagenetic features
Middle Sola Formation	4b, 4y	Massive mudstone texture Well-preserved nannofossil debris	Submicron-sized pyrite
Middle Sola Formation	4c, 5c	Laminated mudstone texture. Variation in clay content. Well-preserved nannofossil debris. Quartz silt	Pyrite crystals location follows lamination Some framboids Rare other sulphides
Lower Sola Formation	2a (clay-rich), 5a, 2b, 3b, 5b, 5y, 2z	Massive mudstone texture. Well-preserved nannofossil debris. Quartz, feldspar and kaolinitic claystone silt. Bioclasts	Submicron-sized and 10 micron sized pyrite Calcite-rimmed dolomite crystals with TiO_2
Lower Sola Formation	5c	Laminated mudstone texture. Variation in clay content. Well-preserved nannofossil debris Kaolinitic claystone silt	
Upper Tuxen Formation	1a	Massive mudstone texture Nannoconid fragments	Partial recrystallization of calcareous nannofossil debris Recrystallized calcitic microfossil Pyrite-cemented microfossils
Middle Tuxen Formation	1a, 2a (clay-poor), 2b (clay-poor)	Massive mudstone texture	Heavily recrystallized (few biogenic features) pyrite
Middle Tuxen Formation	2a (clay-rich), 4a, 2b (clay-rich), 3b, 5b, 2x, 2y	Massive mudstone texture Sparse microfossils and microfossil debris Quartz and kaolinitic claystone silt	Partially recrystallized nannofossil debris Calcite-rimmed dolomite crystals Microfossil cemented by Fe-bearing calcite, TiO_2 Few submicron-sized pyrite crystals
Middle Tuxen Formation	5c	Laminated mudstone texture Variation in clay content Well-preserved nannofossil debris	
Munk Marl Bed	5c	Laminated mudstone texture. Variation in clay content. Well-preserved nannofossil debris. Quartz and kaolinitic claystone silt	Micron-sized pyrite crystals Locally pyrite framboids
Lower Tuxen Formation	2a (clay-poor), 2b (clay-poor), 3b (clay-poor), 2y, 3y, 2z, 3z	Massive mudstone texture Quartz and kaolinitic claystone silt	Heavily recrystallized (single biogenic features) Calcite-rimmed dolomite crystals
Lower Tuxen Formation	2a (clay-rich) 3a, 4a 2b (clay-rich), 3b (clay-rich)	Massive mudstone texture Quartz silt, kaolinitic claystone silt	Partially recrystallized nannofossil debris Calcite-rimmed dolomite crystals Single pyrite clusters and crystals
Valhall Formation	2a (clay-poor)	Massive mudstone texture	Heavily recrystallized carbonate mud Completely recrystallized microfossils
Valhall Formation	4b	Massive mudstone texture Quartz silt	Partially recrystallized nannofossil debris Single pyrite clusters and crystals Diagenetic kaolinite in intrafossil porosity

which in the Boje-2C well comprises the clay-rich Sola Formation and upper Tuxen Formation (Figs 3, 7E, F, 9A, B, 10A, B, 11A, B, 12A–D, 14E, F, A1(A, B), A2(A–F)). Well-preserved nannofossils are also found in the clay-rich Munk Marl Bed (Fig. A3(F)). The clay-poor lithologies of chalk and slightly marly chalk are mainly present in the Tuxen Formation (Figs 4, 5, 8), although one sample from the generally clay-rich Valhall Formation displays the same lithology (Fig. A2(I, J)). The BSE images indicate how the degree of recrystallization gradually increases with depth, while porosity gradually decreases from around 25% to around 17% (Storebø *et al.* 2022a). The recrystallisation is accompanied by pore-filling ce-

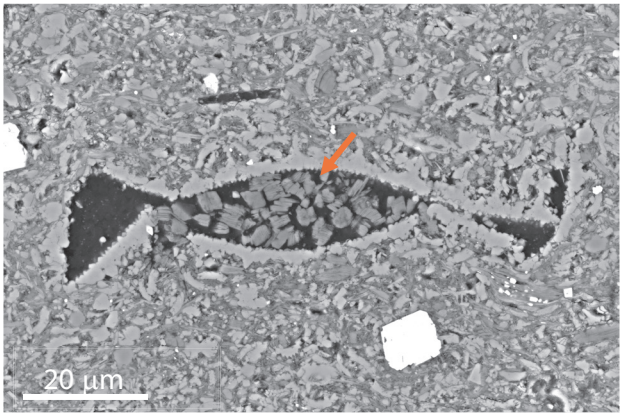


Fig. 16. Backscattered electron micrograph. Diagenetic kaolinite (orange arrow) precipitated in cavity of collapsed microfossil in sample from 8604'2", Valhall Formation, Facies 4b.

mentation, as indicated by the porosity gradient. The calcite is possibly partly sourced from the water zone which was not cored in the Boje-2C well, although pressure dissolution at flaser structures (*sensu lato* solution seams; Garrison & Kennedy 1977; Jelby *et al.* 2022) should also play a role. The difference in calcite cementation between the oil zone and transition zone likely reflects the water saturation at the time of cementation, during which pore space in the upper levels was filled with hydrocarbons and lined with a thin water-film on particle surfaces, while free water dominated the pore space at the deepest levels. Calcite redistribution in the hydrocarbon-bearing interval would then have to have taken place through diffusion in the water film covering the calcite (e.g. Fabricius & Borre 2007).

Burial diagenesis – impact of pressure

During description of the cores from Boje-2C an absence of stylolites was noted (Jelby *et al.* 2022; Glad *et al.* 2022), but flaser structures were observed (*sensu lato* solution seams; Garrison & Kennedy 1977; Jelby *et al.* 2022). Although distinct pressure dissolution features at clay-calcite contacts are not obvious in SEM images (Fig. 13), pressure dissolution may well play a role during the burial diagenesis. In deep sea calcareous sediments, pressure dissolution has been found to take place when the calcite crystals are elastically strained to ~0.003 (Fabricius 2020). (The in situ elastic strain can be calculated from burial depth, bulk density and elastic wave velocity). In deep-sea calcareous pelagic sediments, this strain is reached twice during burial: The first time occurs at the transition from carbonate ooze to chalk, where pressure dissolution causes contact cementation and a drop in strain due to increased particle contact area. In the contact-cemented, carbonate-rich intervals of Boje-2C elastic strain is accordingly around 0.001 (Fabricius & Meireles 2025). The second time pressure dissolution sets in, happens after dispersed clay has recrystallized into clay-rich laminae (Lind 1993; Fabricius & Borre 2007). The dissolved carbonate precipitates as pore-filling cement and no contact cement binds clay and calcite, so strain remains high at this interface and pressure dissolution can continue. In pelagic chalks with low clay content, proper stylolites form (Lind 1993), whereas in more clay-rich pelagic carbonates, a higher density of clay-rich laminae arises and flaser structures develop (Sigurdsson *et al.* 1997; Fabricius 2000). The presence of flaser structures in Boje-2C thus shows that although Boje-2C is overpressured, the pore pressure is not high enough to prevent pressure dissolution.

Silicification and diagenetic kaolinite

Macroscopically evident silicification is not readily identified in the BSE images, probably because silicification is not always pervasive (Fig. 15A) and in some cases only with difficulty noted as aggregates of micro-silica (Fig. 15B).

In a single case, silicification appears as pore-filling cement (Fig. 15), where the silica may have been sourced from siliceous fossils dissolved where the prevalent possible moulds are seen (Figs 10–13). The amorphous appearance of the silica indicates that it may have precipitated as opal-CT, which has later recrystallized to quartz.

Single particles of kaolinite are observed widely in clay-bearing samples and may generally be assumed to be detrital, but some of the particles may have a diagenetic origin, as exemplified by a single case where diagenetic kaolinite was noticed in the intrafossil porosity of a collapsed microfossil (Fig. 16).

Conclusions

A total of 66 samples were analysed in the Lower Cretaceous Tuxen and Sola formations in the cored section of the Boje-2C well (Boje Field, Danish Central Graben, North Sea) through backscatter electron microscopy to delineate how the microscopic character reflects previously recorded macroscopic sedimentary facies and to identify indications of diagenesis. The samples are dominated by calcareous nannofossils, microscopic calcite particles, varying concentrations of presumably detrital clay minerals, minor detrital quartz and kaolinitic claystone (silt) and diagenetic components (calcite cement, silica, pyrite, dolomite). Some of the microscopic calcite particles are clearly derived from nannoconids.

Microfossils are remarkably sparse and particles attributable to benthic fossils are virtually absent.

Porosity is dominantly inter-particular with subordinate intra-particle porosity mainly occurring within nannoconids and less frequently moulds.

In clay-rich samples, kaolinite clay is typically the supporting mineral and calcite particles are separate, embedded in clay. In more calcite-rich samples, calcite particles are in full contact (cemented) and with depth tend to increase in angularity of shape. Pore-filling cementation is found in the deepest samples. The depth-dependant differences in calcite cementation are attributed to the early emplacement of hydrocarbons, which left free water in deeper levels, where cementation took place, while water occurred as film on particles in upper levels where cementation is less prevalent.

Some macroscopic features, such as biomottling and parallel lamination, are clearly reflected in the microscopic texture, whereas shear deformation is indistinguishable from homogeneous bioturbation. By contrast, macroscopically parallel-laminated marlstone of the Munk Marl Bed locally appears microscopically shear-deformed.

Acknowledgements

We gratefully acknowledge the Danish Underground Consortium (TotalEnergies E&P Denmark, BlueNord and Nordsøfonden) for granting permission to publish this work. The study was funded by the Danish Offshore Technology Centre (DTU Offshore). MEJ also acknowledges the Carlsberg Foundation for granting an Internationalisation Fellowship (CF22-0122) and Reintegration Fellowship (CF24-1960), during which this work was partly undertaken. Rikke Weibel and an anonymous reviewer are thanked for constructive comments which helped improve the outcome of this paper. Backscatter micrographs not included in the present paper are available from ILF and KA.

References

Anderskouv, K. & Surlyk, F. 2012: The influence of depositional processes on the porosity of chalk. Journal of the Geological Society 169, 311–325. https://doi.org/10.1144/0016-76492011-079

Blok, C.N., Ineson, J., Anderskouv, K., Fantasia, A., Sheldon, E., Thibault, N., Jelby, M.E., Adatte, T. & Bodin, S. 2022: Latitude dependant climate changes across the Aptian Oceanic Anoxic Event 1a. Palaeogeography, Palaeoclimatology, Palaeoecology 601, 111085. https://doi.org/10.1016/j.palaeo.2022.111085

Blok, C.N., Adatte, T., Ineson, J.R., Sheldon, E., Jelby, M.E., Smit, F.W.H., Lauridsen, B.W., Anderskouv, K. & Bodin, S. 2023.: Clay mineral assemblages as a tool in source-to-sink studies: an example from the Lower Cretaceous of the North Sea Basin. Bulletin of the Geological Society of Denmark, 71, 99–113. https://doi.org/10.37570/bgsd-2023-71-06

Copestake, P., Sims, A.P., Crittenden, S., Hamar, G.P., Ineson, J.R., Rose, P.T. & Tringham, M.E. 2003: Lower Cretaceous. In: Evans, D. et al. (eds): The Millennium Atlas: petroleum geology of the central and northern North Sea. The Geological Society, London, 191–211.

Damtoft, K., Nielsen, L.H., Johannessen, P.N., Thomsen, E. & Andersen, P.R. 1992: Hydrocarbon plays of the Danish Central Trough. In: Spencer, A.M. (ed.): Generation, accumulation and production of Europe's hydrocarbons II, 35–58. Special Publication of the European Association of Petroleum Geoscientists, Springer-Verlag, Berlin. https://doi.org/10.1144/0061331

Eberli, G.P., Swart, P.K., McNeill, D.F., Kenter, J.A.M., Anselmetti, F.S., Melim, L.A. & Ginsburg, R.N. 1997: A synopsis of the Bahamas Drilling Project: results from two deep core borings drilled on the Great Bahama Bank. In: Eberli, G.P., Swart, P.K., Malone, M.J. et al. (eds): Proceedings of the Ocean Drilling Program, Initial Reports 166, 23–41. College Station, TX. https://doi:10.2973/odp.proc.ir.166.103.1997

Fabricius, I.L. 2000: Interpretation of burial history and rebound from loading experiments and the occurence of microstylolites in the mixed sediments of the Caribbean Sites 999 and 1001. In: Leckie, R.M., Sigurdsson, H., Acton, G.D. & Draper, G. (eds): Proceedings of the Ocean Drilling Program, Scientific Results 165, 177–190. College Station, TX. https://doi:10.2973/odp.proc.sr.165.006.2000

Fabricius I.L. 2020: Porosity in chalk – roles of elastic strain and plastic strain. Sedimentology 67, 3451–3470. https://doi:10.1111/sed.12750.

Fabricius, I.L. & Borre, M.K. 2007: Stylolites, porosity, depositional texture, and silicates in chalk facies sediments. Ontong Java Plateau – Gorm and Tyra fields, North Sea. Sedimentology 54, 183–205. https://doi.org/10.1111/j.1365-3091.2006.00828.x

Fabricius, I.L., Olsen, C. & Prasad, M. 2005: Log interpretation of marly chalk, the Lower Cretaceous Valdemar Field, Danish North Sea: application of iso-frame and pseudo water film concepts. The Leading Edge 24, 496–505. https://doi.org/10.1190/1.1926807

Fabricius, I.L. & Meireles, L.T.P. 2025. Assessment of pore collapse in North Sea Lower Cretaceous carbonates using downhole elastic strain. Bulletin of the Geological Society of Denmark, 71, 115–125. https://doi.org/10.37570/bgsd-2025-71-07

Gale, A.S., Mutterlose, J., Batenburg, S., Gradstein, F.M., Agterberg, F.P., Ogg, J.G. & Petrizzo, M.R. 2020: The Cretaceous Period. In: Gradstein, F.M., Ogg, J.G., Schmitz, M.D. and Ogg, G.M. (eds): Geological Time Scale 2020, 1023–1086. Boston: Elsevier. https://doi.org/10.1016/b978-0-12-824360-2.00027-9

Garrison, R.E. & Kennedy, W.J. 1977: Origin of solution seams and flaser structure in Upper Cretaceous chalks of southern England. Sedimentary Geology 19, 107–137. https://doi.org/10.1016/0037-0738(77)90027-6

Glad, A.C., Amour, F., Welch, M.J., Clausen, O.R., Anderskouv, K., Ineson, J.R., Sheldon, E. & Nick, H.M. 2022: Natural fractures and discontinuities in a Lower Cretaceous chalk-marlstone reservoir, Valdemar Field, Danish North Sea. Marine and Petroleum Geology 136, 105445. https://doi.

org/10.1016/j.marpetgeo.2021.105445
Hesselbo, S.P., Ogg, J.G., Ruhl, M., Hinnov, L.A. & Huang, C.J. 2020: The Jurassic Period. In: Gradstein, F.M., Ogg, J.G., Schmitz, M.D. and Ogg, G.M. (eds): Geological Time Scale 2020, 955–1021. Boston: Elsevier. https://doi.org/10.1016/b978-0-12-824360-2.00026-7
Ineson, J.R. 1993: The Lower Cretaceous chalk play in the Danish Central Trough. In: Parker, J.R. (ed.): Petroleum Geology of Northwest Europe: Proceedings of the 4th Conference, 175–183. Geological Society, London. https://doi.org/10.1144/0040175
Ineson, J.R., Lauridsen, B.W., Lode, S., Sheldon, E., Sørensen, H.O., Wisshak, M. & Anderskouv, K. 2022a: A condensed chalk–marl succession on an Early Cretaceous intrabasinal structural high, Danish Central Graben: Implications for the sequence stratigraphic interpretation of the Munk Marl Bed. Sedimentary Geology, 440, 106234. https://doi.org/10.1016/j.sedgeo.2022.106234
Ineson, J.R., Petersen, H.I., Andersen, C., Bjerager, M., Jakobsen, F.C., Kristensen, L., Mørk, F. & Sheldon, E. 2022b: Early Cretaceous stratigraphic and basinal evolution of the Danish Central Graben: a review. Bulletin of the Geological Society of Denmark, 71, 75–98. https://doi.org/10.37570/bgsd-2022-71-05
Jakobsen, F., Ineson, J.R., Kristensen, L. & Stemmerik, L. 2004: Characterization and zonation of a marly chalk reservoir: the Lower Cretaceous Valdemar Field of the Danish Central Graben. Petroleum Geoscience 10, 21–33. https://doi.org/10.1144/1354-079303-584
Jakobsen, F., Ineson, J.R., Kristensen, L., Nytoft, H.P. & Stemmerik, L. 2005: The Valdemar Field, Danish Central Graben: field compartmentalization and regional prospectivity of the Lower Cretaceous chalk play. In: Doré, A.G. & Vining, B.A. (eds): Petroleum Geology: North-West Europe and Global Perspectives—Proceedings of the 6th Petroleum Geology Conference, 177–186. Geological Society, London. https://doi.org/10.1144/0060177
Japsen, P., Britze, P. & Andersen, C. 2003: Upper Jurassic – Lower Cretaceous of the Danish Central Graben: structural framework and nomenclature. Geological Survey of Denmark and Greenland Bulletin 1, 233–246. https://doi.org/10.34194/geusb.v1.4653
Jelby, M.E., Ineson, J.R., Thibault, N., Bodin, S., Blok, C.N., Edvardsen, N., Clemmensen, T.S., Buls, T. & Anderskouv, K. 2022: Facies and depositional processes of Lower Cretaceous carbonates, Danish Central Graben. Bulletin of the Geological Society of Denmark 71, 51–74. https://doi.org/10.37570/bgsd-2022-71-04
Jelby, M.E., Ineson, J.R., Sheldon, E. & Anderskouv, K. 2024: Old chalk, new tricks: revisiting the Lower Cretaceous carbonates of the Danish Central Graben. In: Hart, M.B., Batenburg, S.J., Huber, B.T., Price, G.D., Thibault, N., Wagreich, M. & Walaszczyk, I. (eds): Cretaceous Project 200 Volume 2: Regional Studies. Geological Society, London, Special Publications 545. https://doi.org/10.1144/sp545-2023–134
Jensen, T.F. & Buchardt, B. 1987: Sedimentology and geochemistry of the organic carbon-rich Lower Cretaceous Sola Formation (Baremian–Albian), Danish North Sea. In: Brooks, J. & Glennie, K. (eds): Petroleum Geology of North-West Europe, 431–440. Graham & Trotman.
Jensen, T.F., Holm, L., Frandsen, N. & Michelsen, O. 1986: Jurassic - Lower Cretaceous lithostratigraphic nomenclature for the Danish Central Trough. Danmarks Geologiske Undersøgelse, Serie A, 12, 64 pp. https://doi.org/10.34194/seriea.v12.7031
Kühnau, L. & Michelsen, O. 1994: Detailed log-stratigraphic study of the Lower Cretaceous in the Danish Central Trough, North Sea. Marine and Petroleum Geology 11, 467–477. https://doi.org/10.1016/0264-8172(94)90080-9Get rights and content
Lauridsen, B.W., Lode, S., Sheldon, E., Frykman, P., Anderskouv, K. & Ineson, J. 2022: Lower Cretaceous (Hauterivian–Aptian) pelagic carbonates in the Danish Basin: new data from the Vinding-1 well, central Jylland, Denmark. Bulletin of the Geological Society of Denmark, 71, 7–29. https://doi.org/10.37570/bgsd-2022-71-02
Lind, I.L. 1993: Stylolites in chalk from Leg 130, Ontong Java Plateau. Proceedings of the Ocean Drilling Program, Scientific Results 130, 445–451. College Station, TX. https://doi.org/10.2973/odp.proc.sr.130.006.1993
Meireles, L.T.P. &. Fabricius, I.L. 2023: Deriving mineral moduli of the noncarbonate fraction in a marly chalk reservoir using petrophysical logging data and an isoframe model. Geophysics 88, D411–D425. https://doi.org/10.1190/geo2022-0493.1
Michelsen, O., Frandsen, N., Holm, L., Jensen, T.F., Møller, J.J. & Vejbæk, O.V. 1987: Jurassic - Lower Cretaceous of the Danish Central Trough; – depositional environments, tectonism, and reservoirs. Danmarks Geologiske Undersøgelse, Serie A, 16, 44 pp. https://doi.org/10.34194/seriea.v16.7035
Møller, J.J. & Rasmussen, E.S. 2003: Middle Jurassic – Early Cretaceous rifting of the Danish Central Graben. Geological Survey of Denmark and Greenland Bulletin 1, 247–264. https://doi.org/10.34194/geusb.v1.4654
Musgrave, R.J., Delaney, M.L., Stax, R. & Tarduno, J.A. 1993: Magnetic diagenesis, organic input, interstitial water chemistry, and palaeomagnetic record of the carbonate sequence of the Ontong Java Plateau. Proceedings of the Ocean Drilling Program, Scientific Results 130, 527–546.
Mutterlose, J. 1992: Migration and evolution patterns of floras and faunas in marine Early Cretaceous sediments of NW Europe. Palaeogeography, Palaeoclimatology, Palaeoecology 94, 261–282. https://doi.org/10.1016/0031-0182(92)90123-M
Mutterlose, J. & Bottini, C. 2013: Early Cretaceous chalks from the North Sea giving evidence for global change. Nature Communications 4, 1686.
Petersen, H.I. & Jakobsen, F.C. 2021: Lithostratigraphic definition of the Upper Jurassic – lowermost Cretaceous (upper Volgian–Ryazanian) organic-rich and oil-prone Mandal Formation in the Danish Central Graben, North Sea. Marine and Petroleum Geology, 129, 105116. https://doi.org/10.1016/j.marpetgeo.2021.105116
Sigurdsson, H., Leckie, R.M., Acton, G.D. et al. 1997: Proceedings of the Ocean Deep Drilling Project, Initial Reports 165: College Station, TX (Ocean Drilling Program). https://doi:10.2973/odp.proc.ir.165.1997
Storebø, E.M., Meireles, L.T.P. & Fabricius, I.L. 2022a: Permeability modelling in clay-rich carbonate. Petrophysics 63, 148–171. https://doi: 10.30632/PJV63N2-2022a2

Storebø, E.M., Hjuler, M.L., Meireles, L.T.P. & Fabricius, I.L. 2022b: Effect of pyrite in water saturation evaluation of clay-rich carbonate. Petrophysics 63, 172–198. https://doi: 10.30632/PJV63N2-2022a3

Tagliavento, M., John, C.M., Anderskouv, K. & Stemmerik, L. 2021: Towards a new understanding of the genesis of chalk: Diagenetic origin of micarbs confirmed by clumped isotope analysis. Sedimentology 68, 513–530. https://doi.org/10.1111/sed.12802

Tyson, R.V. & Funnell, B.M. 1987: European Cretaceous shorelines, stage by stage. Palaeogeography, Palaeoclimatology, Palaeoecology 59, 69–91. https://doi.org/10.1016/0031-0182(87)90075-7

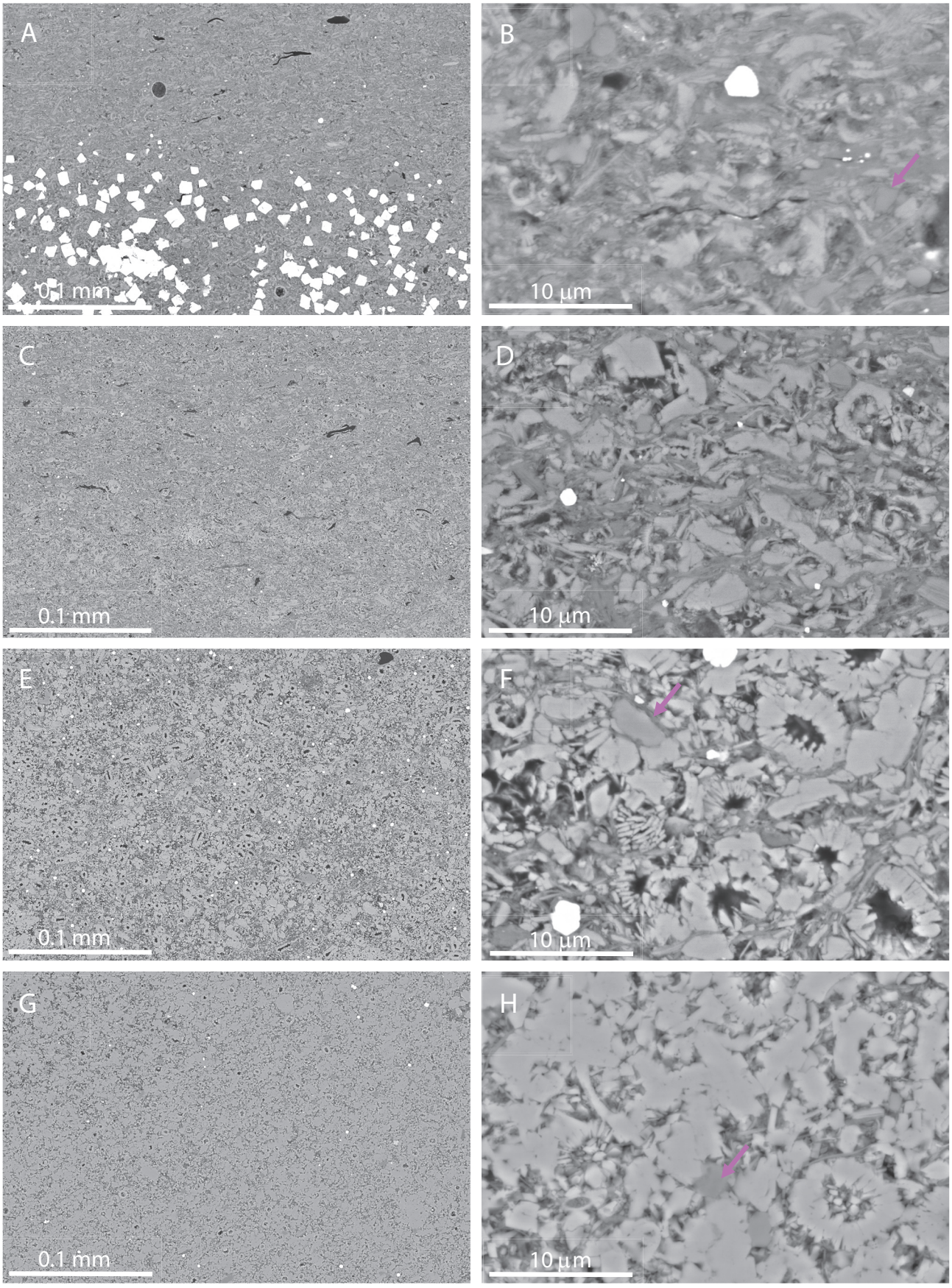
van Buchem, F.S.P., Smit, F.W.H., Buijs, G.J.A., Trudgill, B. & Larsen, P.-H. 2018: Tectonostratigraphic framework and depositional history of the Cretaceous–Danian succession of the Danish Central Graben (North Sea) – new light on a mature area. In: Bowman, M. & Levell, B. (eds): Petroleum Geology of NW Europe: 50 Years of Learning – Proceedings of the 8th Petroleum Geology Conference. Geological Society, London. https://doi.org/10.1144/PGC8.24.

Vejbæk, O.V. 1986: Seismic stratigraphy and tectonic evolution of the Lower Cretaceous in the Danish Central Trough. Danmarks Geologiske Undersøgelse, Serie A, 11, 57 pp. https://doi.org/10.34194/seriea.v11.7030

Vejbæk, O.V. & Andersen, C. 1987: Cretaceous–Early Tertiary inversion tectonism in the Danish Central Trough. Tectonophysics 137, 221–238. https://doi.org/10.1016/0040-1951(87)90321-0

Wennberg, O.P., Casini, G., Jahanpanah, A., Lapponi, F., Ineson, J., Wall, B.G. & Gillespie, P. 2013: Deformation bands in chalk, examples from the Shetland Group of the Oseberg Field, North Sea, Norway. Journal of Structural Geology 56, 103–117. https://doi.org/10.1016/j.jsg.2013.09.005

Appendix


A
0.1 mm
B
10 µm
C
0.1 mm
D
10 µm
E
0.1 mm
F
10 µm
G
0.1 mm
H
10 µm

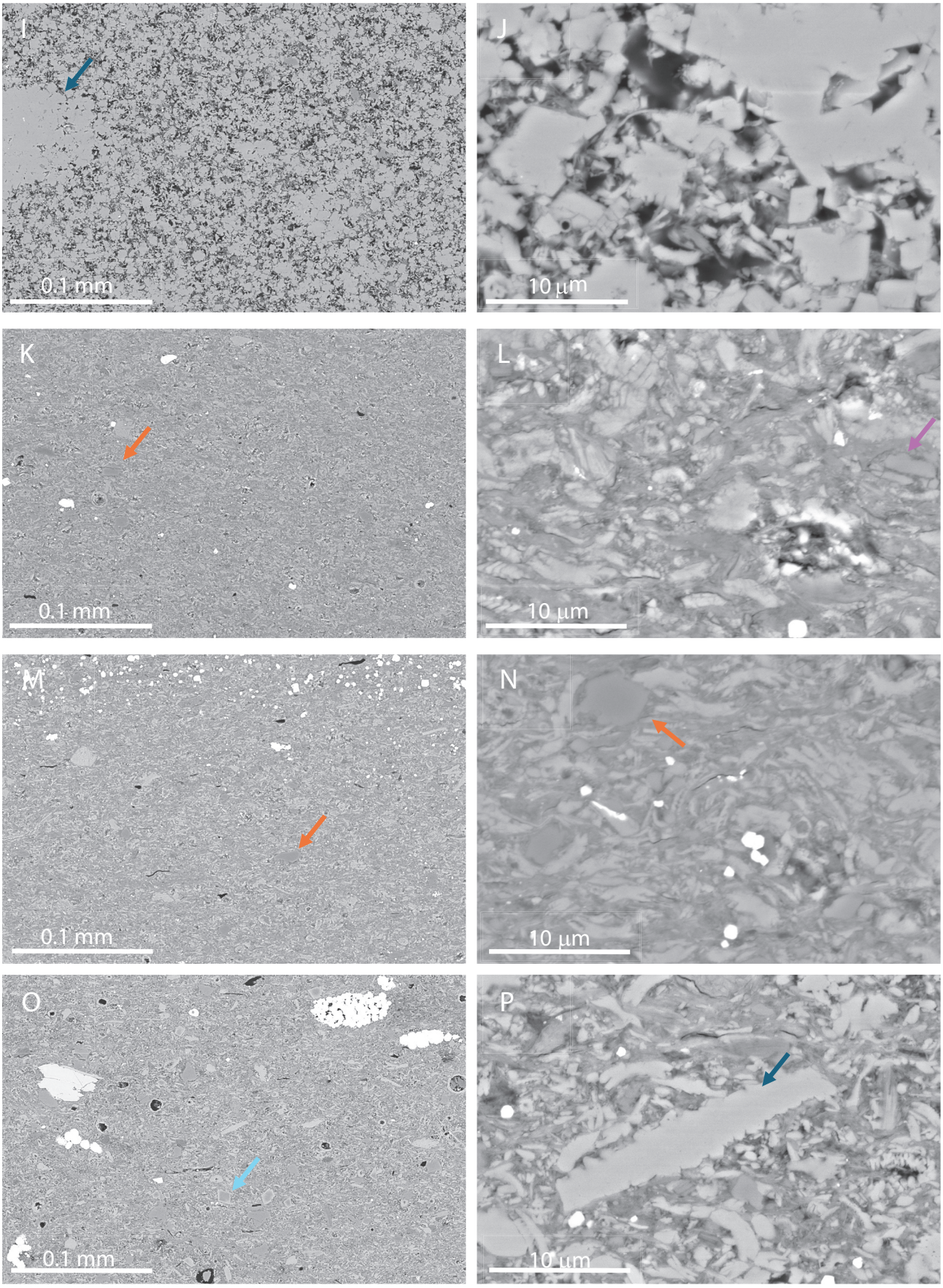
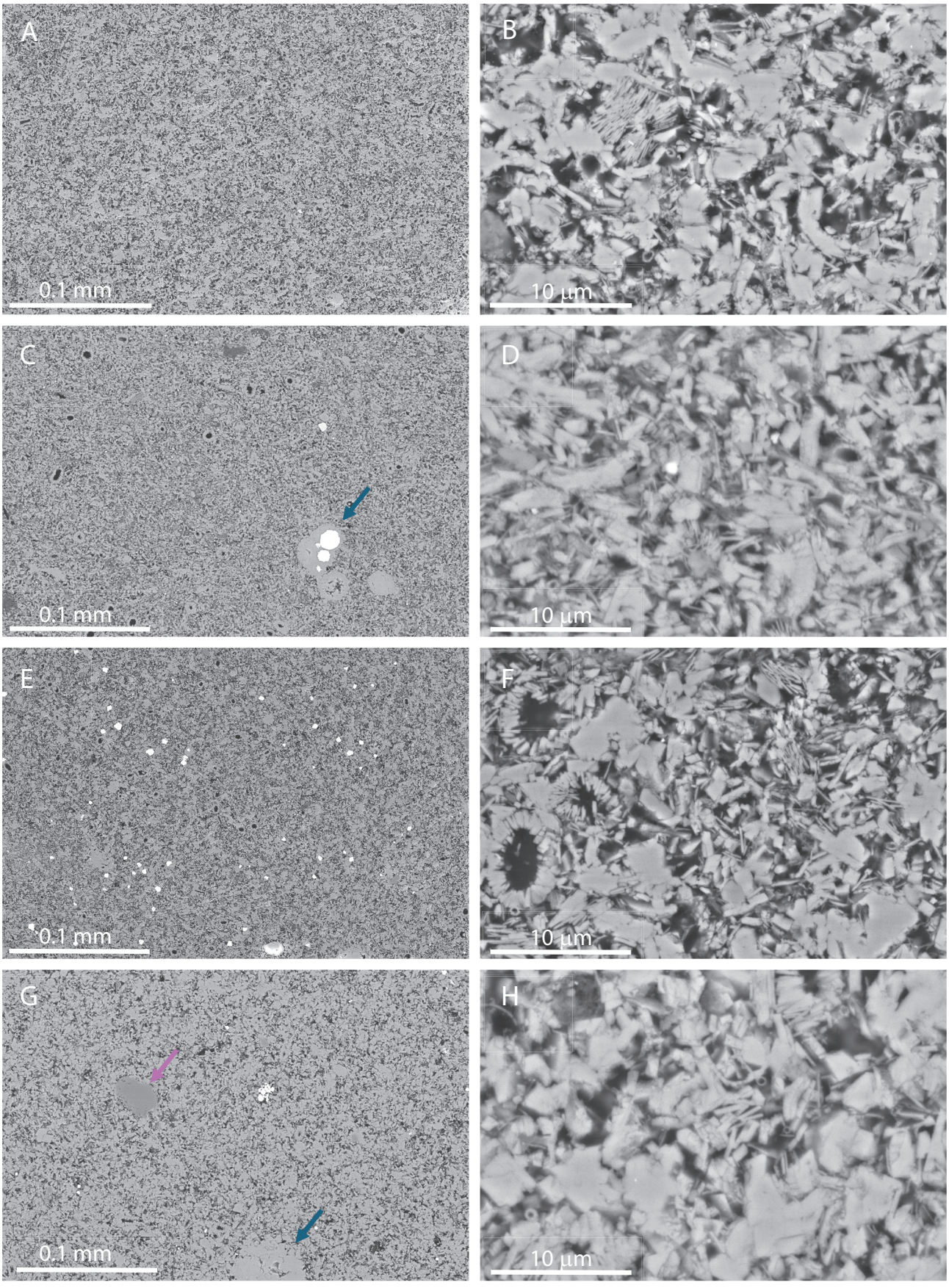
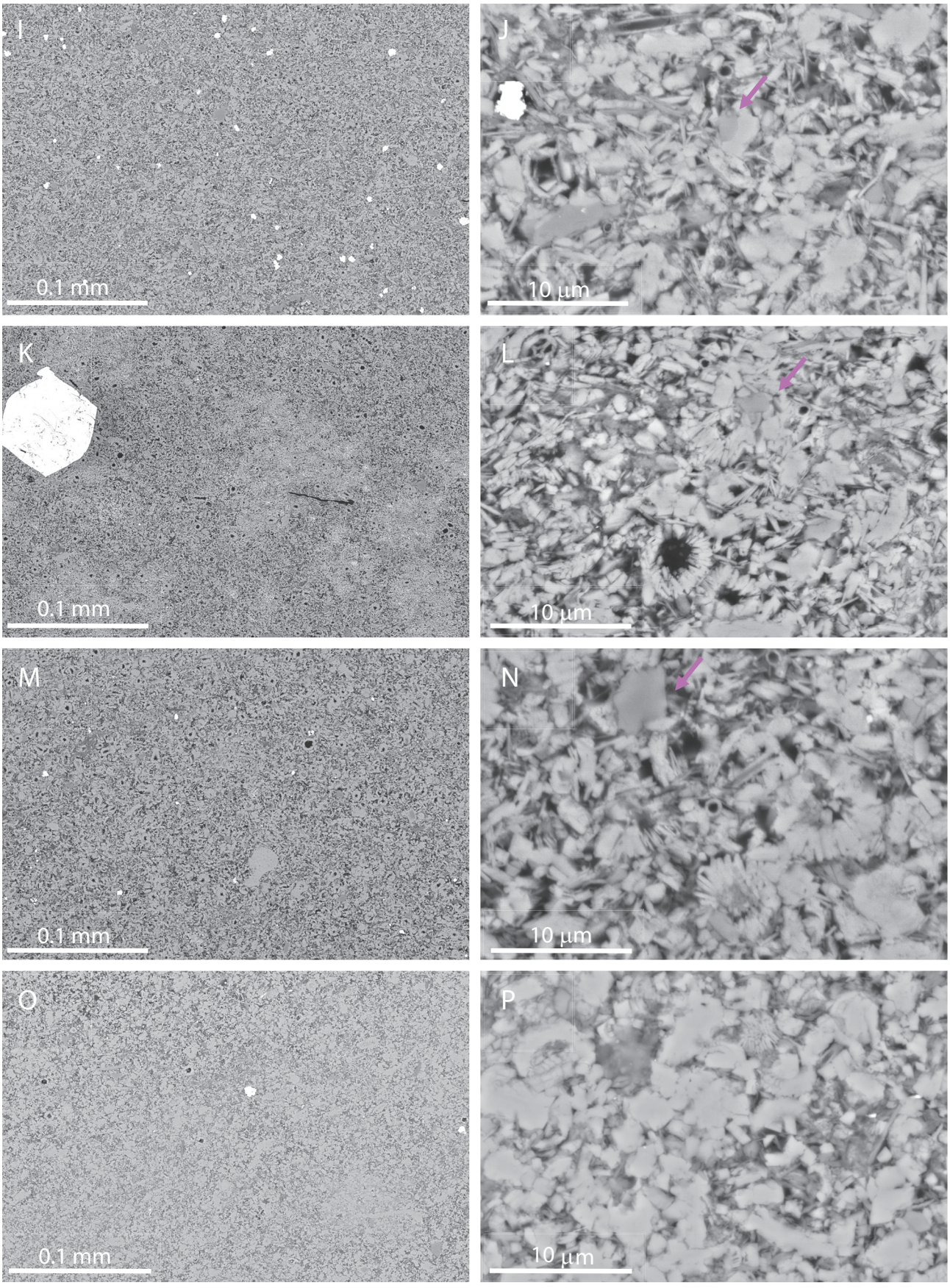
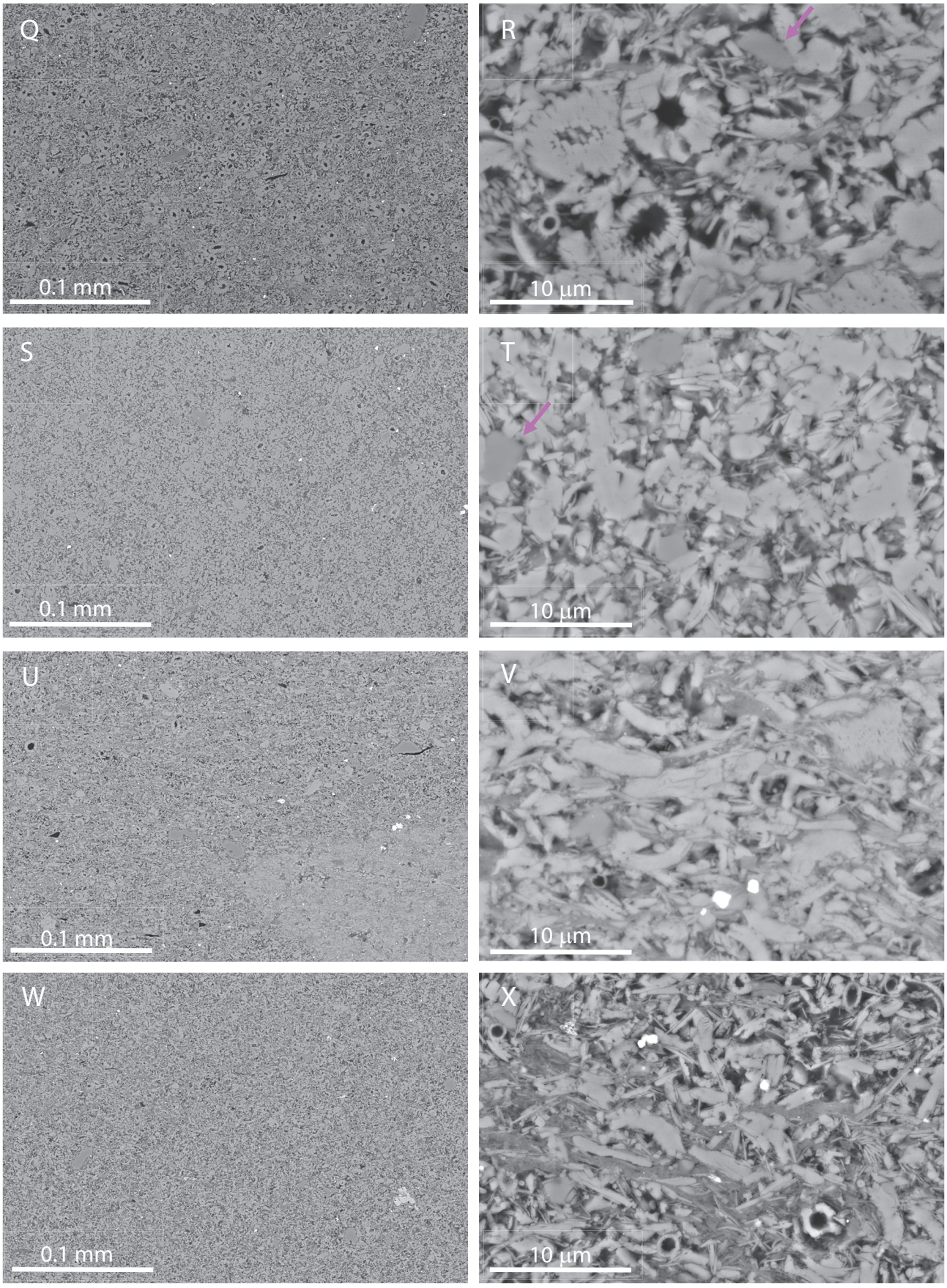
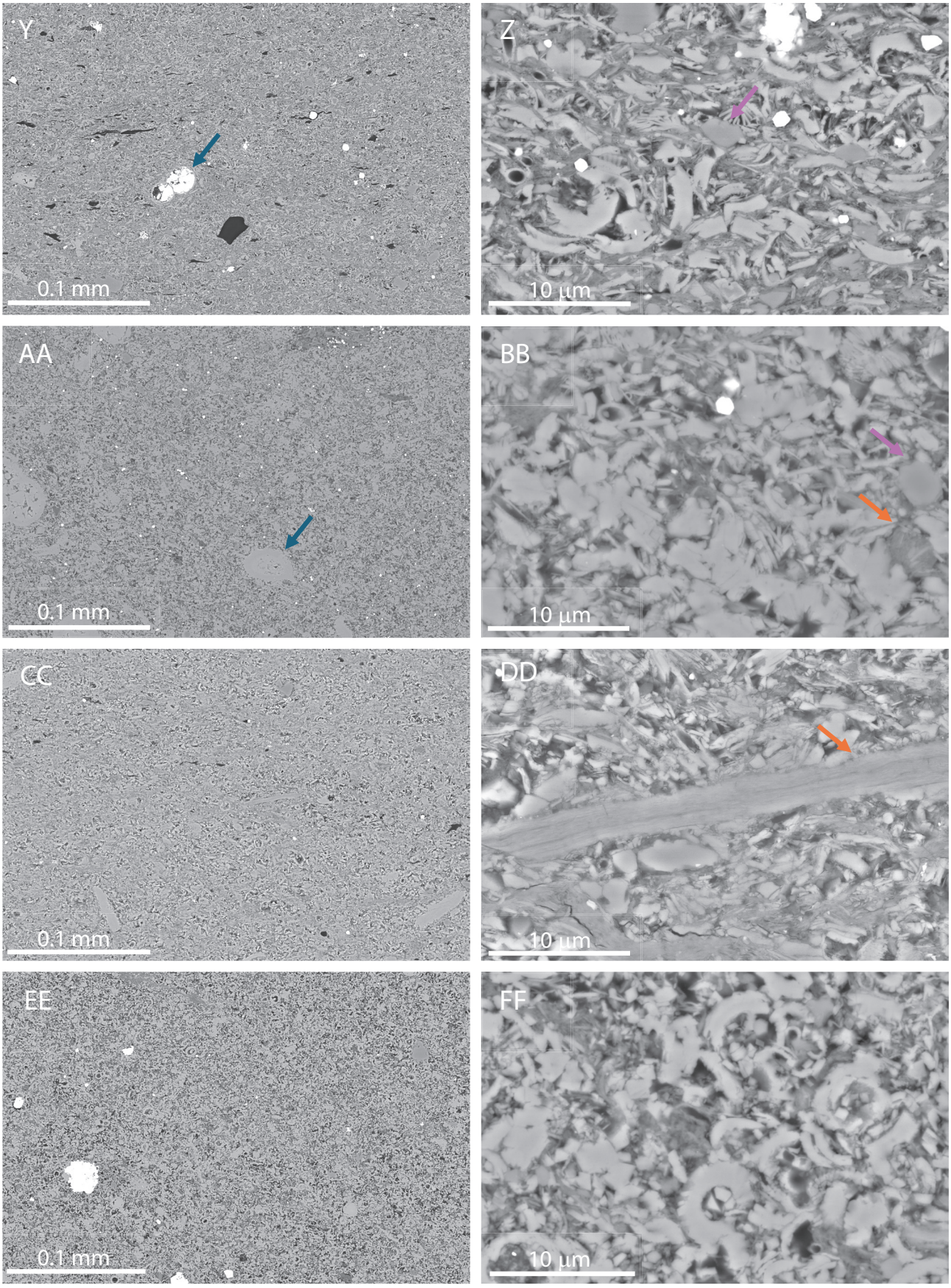

I
0.1 mm
J
10 µm
K
0.1 mm
L
10 µm
M
0.1 mm
N
10 µm
O
0.1 mm
P
10 µm

Fig. A1. Backscattered electron micrographs, illustrating texture (left) and pore geometry (right) of Facies 2a (homogeneously bioturbated slightly marly chalk; **A–J**), Facies 3a (homogeneously bioturbated marly chalk; **K**, **L**) and Facies 4a (homogeneously bioturbated chalky marlstone; **M–P**). (**A**, **B**) Sample from 8379'11'', Lower Sola Formation. (**C**, **D**) Sample from 8469'5'', Middle Tuxen Formation. (**E**, **F**) Sample from 8520', Lower Tuxen Formation. (**G**, **H**) Sample from 8574'10'', Lower Tuxen Formation. (**I**, **J**) Sample from 8607' Valhall Formation. (**K**, **L**) Sample from 8576'1'', Lower Tuxen Formation. (**M**, **N**) Sample from 8475'11'', Middle Tuxen Formation. (**O**, **P**) Sample from 8539'5'', Lower Tuxen Formation. Arrow colours signify: pink: quartz silt, blue: calcite-cemented microfossils, orange: kaolinitic claystone clast, light blue: calcite-rimmed dolomite crystal.


A
0.1 mm
B
10 µm
C
0.1 mm
D
10 µm
E
0.1 mm
F
10 µm
G
0.1 mm
H
10 µm


I
0.1 mm
J
10 µm
K
0.1 mm
L
10 µm
M
0.1 mm
N
10 µm
O
0.1 mm
P
10 µm


Q
0.1 mm
R
10 µm
S
0.1 mm
T
10 µm
U
0.1 mm
V
10 µm
W
0.1 mm
X
10 µm


Y
0.1 mm
Z
10 µm
AA
0.1 mm
BB
10 µm
CC
0.1 mm
DD
10 µm
EE
0.1 mm
FF
10 µm

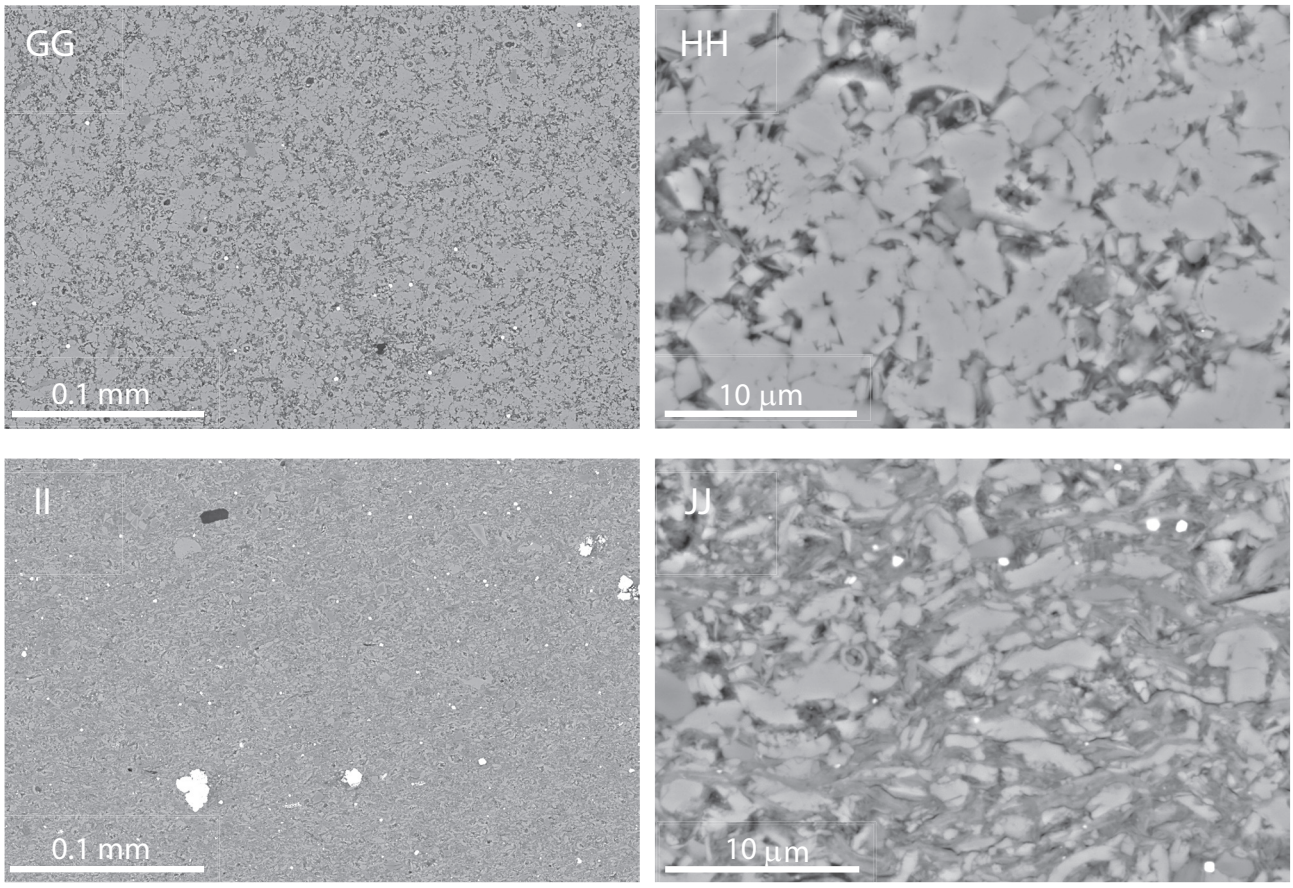
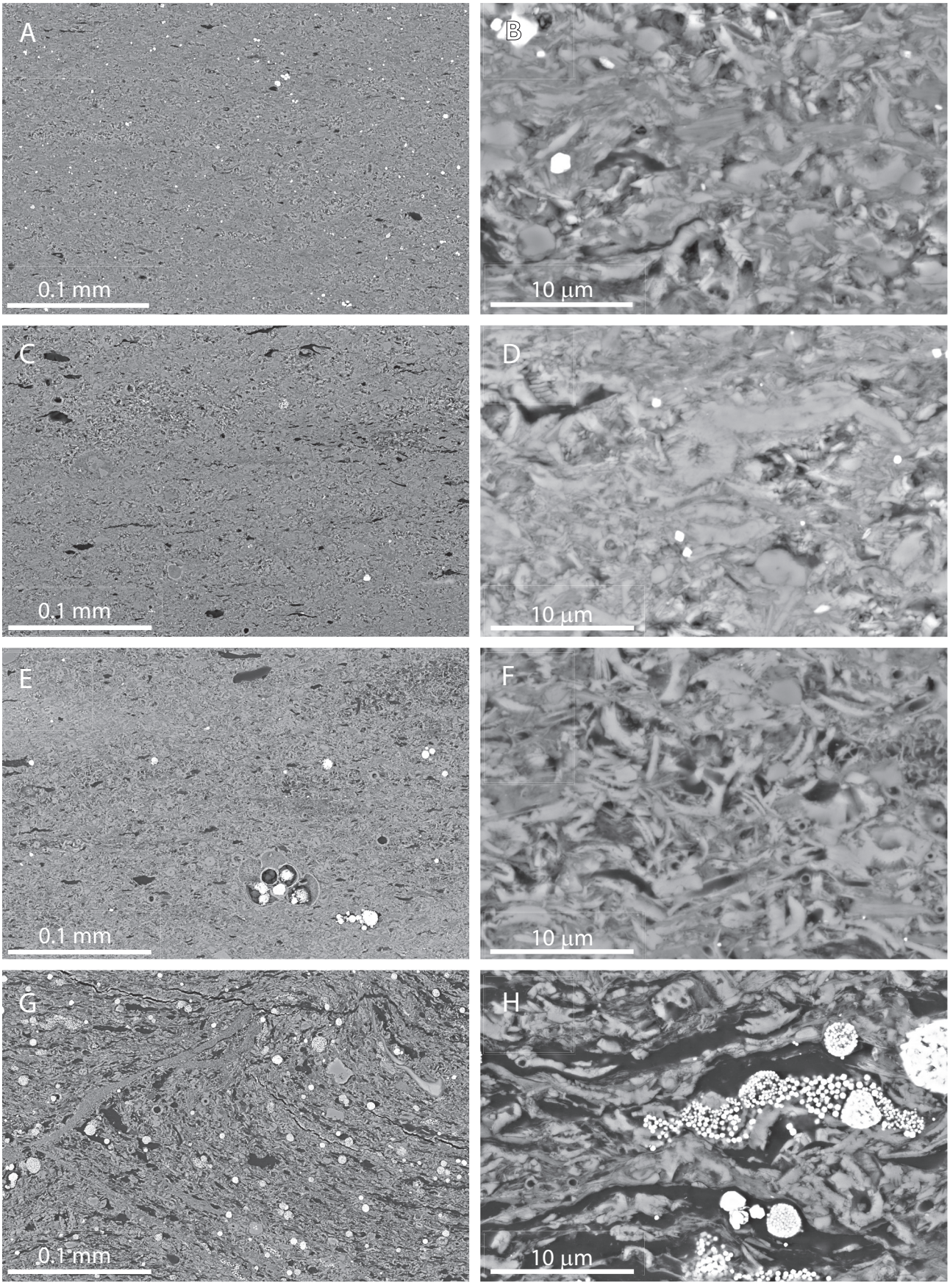


Fig. A2. Backscattered electron micrographs, illustrating texture (left) and pore geometry (right) of Facies 2b (biomottled slightly marly chalk; **A–T**), Facies 3b (biomottled marly chalk; **U–HH**) and Facies 4b (biomottled chalky marlstone; **II, JJ**). (**A**, **B**) Sample from 8390′, Lower Sola Formation. (**C**, **D**) Sample from 8433′1″, Middle Tuxen Formation. (**E**, **F**) Sample from 8459′10″, Middle Tuxen Formation. (**G**, **H**) Sample from 8472′, Middle Tuxen Formation. (**I**, **J**) Sample from 8492′11″, Lower Tuxen Formation. (**K**, **L**) Sample from 8505′, Lower Tuxen Formation. (**M**, **N**) Sample from 8511′1″, Lower Tuxen Formation. (**O**, **P**) Sample from 8512′9″, Lower Tuxen Formation (**Q**, **R**) Sample from 8550′5″, Lower Tuxen Formation. (**S**, **T**) Sample from 8560′, Lower Tuxen Formation. (**U**, **V**) Sample from 8424′11″, Middle Tuxen Formation. (**W**, **X**) Sample from 8450′11″, Middle Tuxen Formation. (**Y**, **Z**) Sample from 8451′11″, Middle Tuxen Formation. (**AA**, **BB**) Sample from 8480′3″, Middle Tuxen Formation. (**CC**, **DD**) Sample from 8485′, Middle Tuxen Formation. (**EE**, **FF**) Sample from 8559′1″, Lower Tuxen Formation. (**GG**, **HH**) Sample from 8566′1″, Lower Tuxen Formation. (**II**, **JJ**) Sample from 8604′2″, Valhall Formation. Arrow colours signify: pink: quartz silt, blue: calcite- and pyrite-cemented microfossils, orange: kaolinitic claystone clast.


A
0.1 mm
B
10 µm
C
0.1 mm
D
10 µm
E
0.1 mm
F
10 µm
G
0.1 mm
H
10 µm

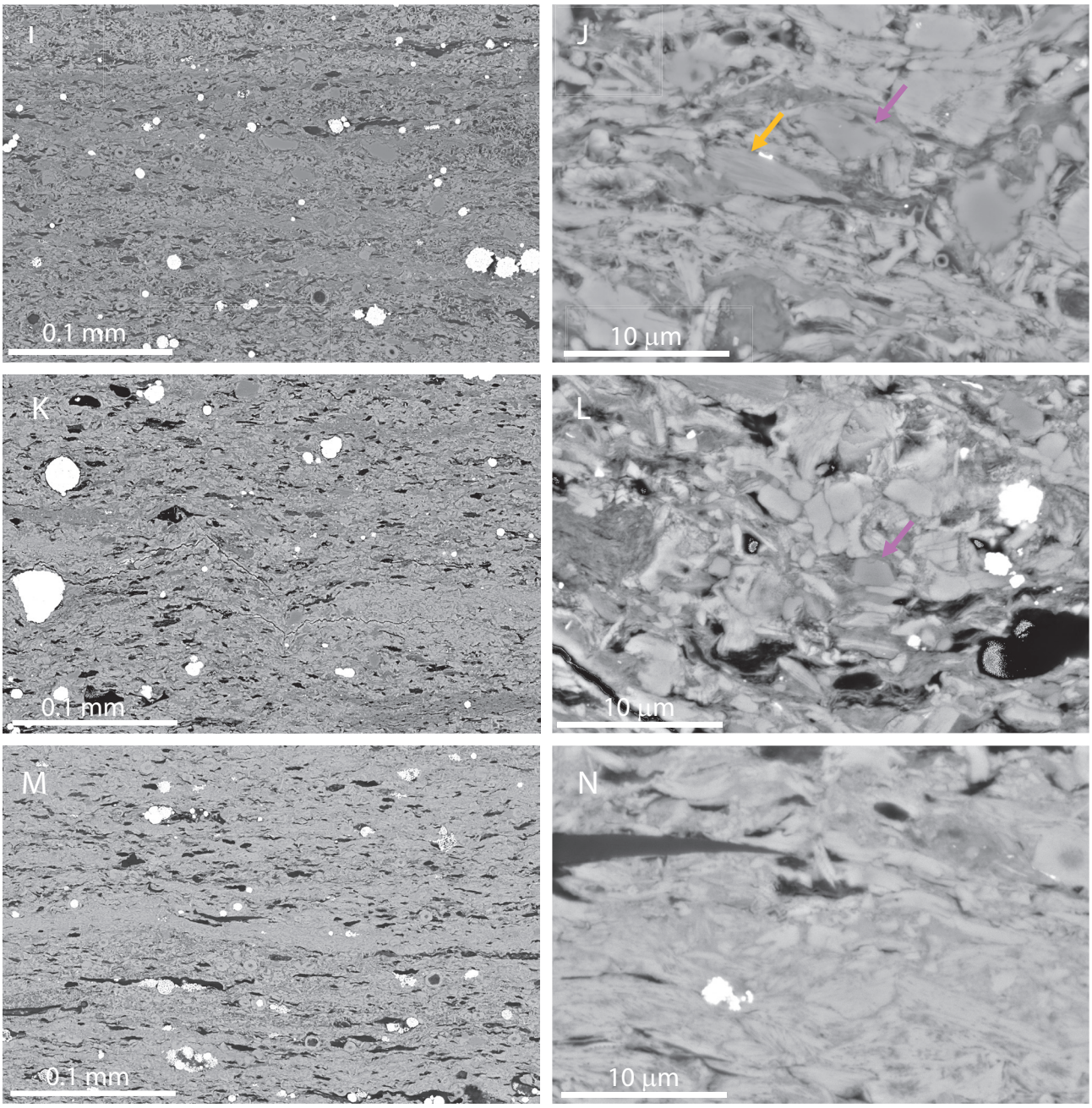
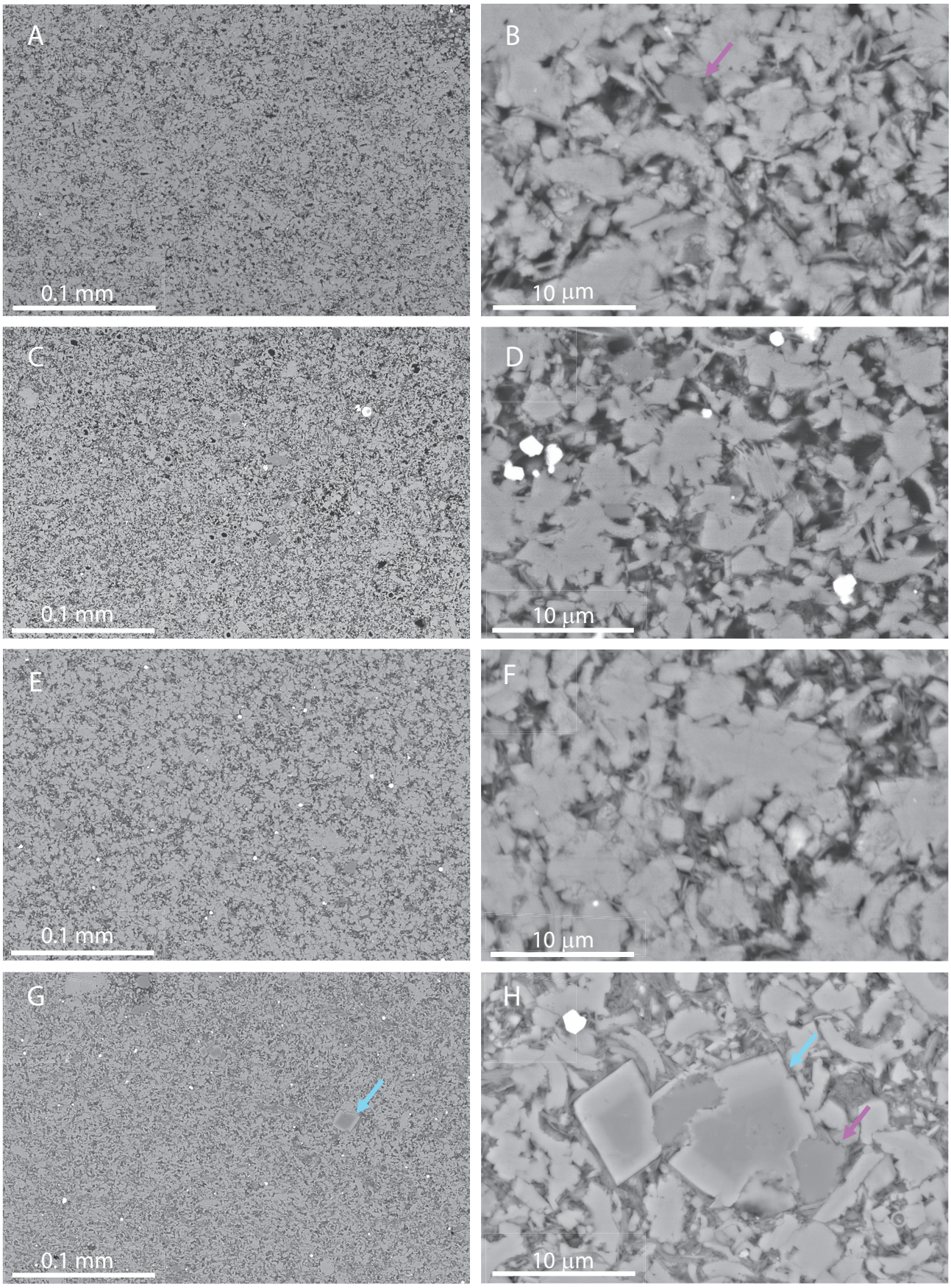


Fig. A3. Backscattered electron micrographs, illustrating texture (left) and pore geometry (right) of Facies 5c (parallel-laminated marlstone). (**A, B**) Sample from 8393'11'', Lower Sola Formation. (**C**, **D**) Sample from 8446'3'', Middle Tuxen Formation. (**E**, **F**) Sample from 8486', Munk Marl Bed. (**G**, **H**) Sample from 8487'1'', Munk Marl Bed. (**I**, **J**) Sample from 8488'4'', Munk Marl Bed. (**K**, **L**) Sample from 8490'3'', Munk Marl Bed. (**M**, **N**) Sample from 8491'1'', Munk Marl Bed. Arrow colours signify: pink: quartz silt, orange: kaolinitic claystone clast.

Fig. A4. Backscattered electron micrographs, illustrating texture (left) and pore geometry (right) of Facies 2y (shear-deformed slightly marly chalk). (**A, B**) Sample from 8515'2'', Lower Tuxen Formation. (**C**, **D**) Sample from 8557'11'', Lower Tuxen Formation. (**E**, **F**) Sample from 8581'1'', Lower Tuxen Formation. (**G**, **H**) Sample from 8582', Lower Tuxen Formation. Arrow colours signify: pink: quartz silt, light blue: calcite-rimmed dolomite crystal.


A
0.1 mm
B
10 µm
C
0.1 mm
D
10 µm
E
0.1 mm
F
10 µm
G
0.1 mm
H
10 µm

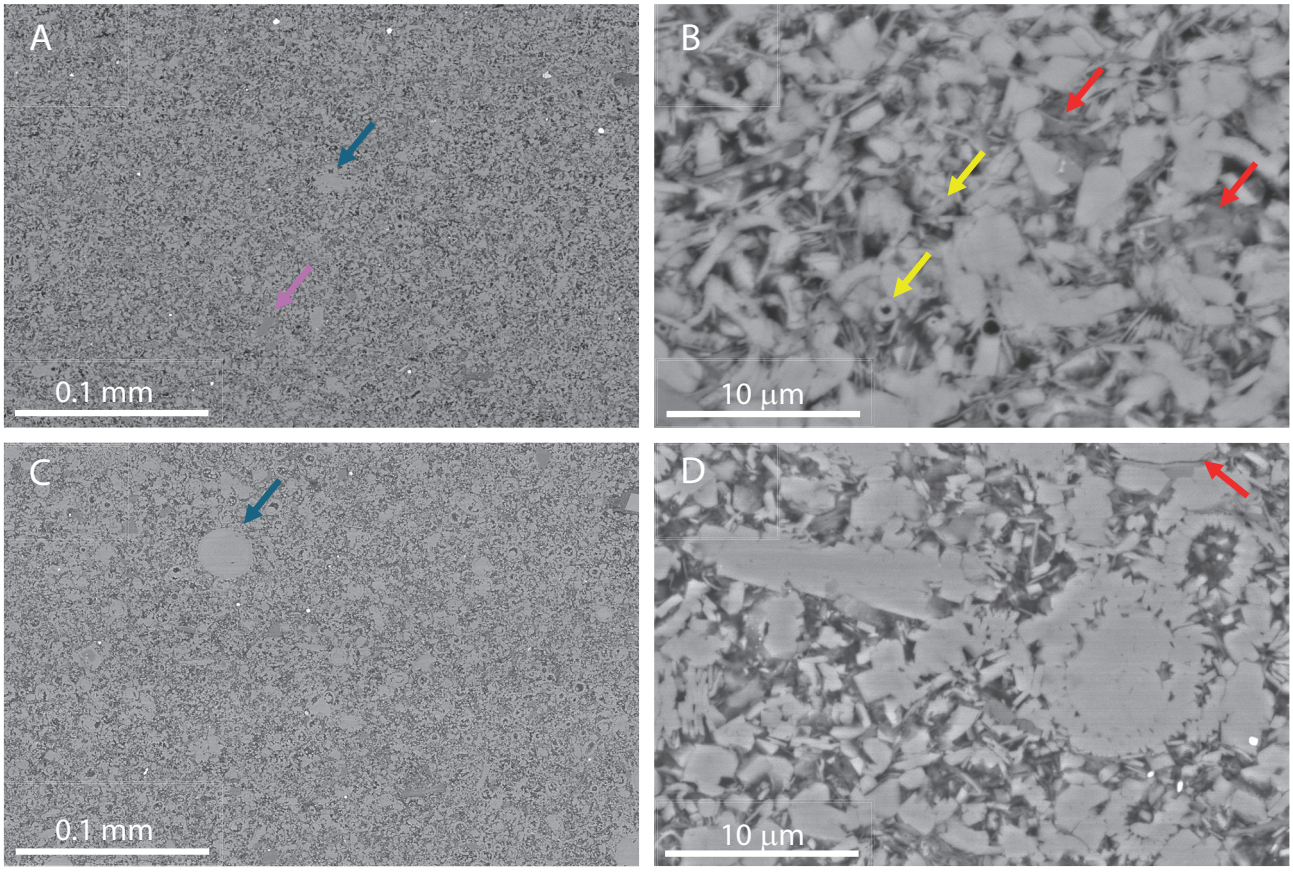


Fig. A5. Backscattered electron micrographs, illustrating texture (left) and pore geometry (right) of Facies 2z (silicified slightly marly chalk). (**A, B**) Sample from 8494'1", Lower Tuxen Formation. (**C**, **D**) Sample from 8541'11", Lower Tuxen Formation. Arrow colours signify: pink: quartz silt, blue: probably cemented calcitic microfossil or fossil clasts, red: possible silica cement.